DNA SEPARATION AT A STRETCH AND MULTISTAGE MAGNETIC SEPARATION OF MICROSPHERES

by

Jiamin Wu

BS, Tongji University, 2000

MS, Beijing University of Chemical Technology, 2003

Submitted to the Graduate Faculty of

Swanson School of Engineering in partial fulfillment

of the requirements for the degree of

Doctor of Philosophy

University of Pittsburgh

2012

UNIVERSITY OF PITTSBURGH

SWANSON SCHOOL OF ENGINEERING

This dissertation was presented

by

Jiamin Wu

It was defended on

November 07, 2012

and approved by

Xinyan Tracy Cui, PhD, Associate Professor, Department of Bioengineering

Steven R. Little, PhD, Associate Professor, Department of Chemical and Petroleum Engineering

Sachin Velankar, PhD, Associate Professor, Department of Chemical and Petroleum Engineering

Dissertation Director: Di Gao, PhD, Associate Professor, Department of Chemical and Petroleum Engineering

DNA SEPARATION AT A STRETCH AND MULTISTAGE MAGNETIC SEPARATION OF MICROSPHERES

Jiamin Wu, PhD

University of Pittsburgh, 2012

This thesis consists of two parts. The first part focuses on development of a novel DNA separation technology by tethering DNA strands to a solid surface and then stretching the DNA with an electric field. The anchor is such designed that the critical force to detach a DNA is independent of its size. Because the stretching force is proportional to the DNA net charge, a gradual increase of the electric field leads to size-based removal of the DNA from the surface and thus DNA separation. This strategy may provide a convenient, low-cost, and high-speed alternative to existing methods for DNA separation, because sieving matrices are not required, separated DNA can be readily recovered, and in principle, there is no upper limit on the length of DNA that can be separated. Using this method, we have demonstrated (i) efficient separation of lambda double-stranded DNA (dsDNA) (48,502 bp) from human genomic dsDNA (>100 kbp) in a dc electric field applied between two parallel plates, (ii) separation of short single-stranded DNA (ssDNA) with less than 100 nucleotides (nt) at 10-nt resolution by tethering and stretching DNA in microfluidic channels filled with a low conductivity buffer, and (iii) separation of short ssDNA by taking the advantage of the strong yet evolving non-uniform electric field near the charged Au surface in contact with an electrolyte.

The second part of my thesis focuses on development of a multistage separation technology to circumvent the challenge caused by non-specific interactions in current single-stage magnetic separation techniques. The key idea is to allow the magnetic particles (MNPs) to

reversibly capture and release the targets by manipulating the hydrophobic interaction between the MNPs and the targets. This will be enabled by attaching temperature-responsive polymers to both the MNPs and the targets. Through temperature cycling, which triggers the reversible hydrophilic-to-hydrophobic phase transition of the polymers, the targets can be reversibly captured and released by the MNPs (due to hydrophobic interaction) at a higher efficiency than the non-targets which may also be captured and released by the MNPs due to non-specific interactions. The difference in the capture-and-release efficiencies of targets versus non-targets in a single cycle will be amplified by multiple separation stages, following a similar concept to the distillation process. As a proof-of-concept demonstration, we have demonstrated efficient separation of poly(N-isopropylacrylamide) (PNIPAM, a temperature responsive polymer)-functionalized polystyrene (PS) microspheres from bare PS microspheres by using PNIPAM-functionalized MNPs. The overall enrichment factor is observed to significantly increase with the number of separation stages, and reaches as high as 1.87×10^5 after 5 stages.

TABLE OF CONTENTS

LIST OF TABLES

LIST OF FIGURES

ACKNOWLEDGMENTS

This dissertation would be absolutely impossible without helping hands of many individuals. I would like to express my sincerest gratitude to my PhD advisor, Prof. Di Gao for being a wonderful mentor. His continuous encouragement and support during this research have enabled me to explore various emerging research areas. I would like to thank my advisory committee members Prof. Tracy Cui, Prof. Steven Little, and Prof. Sachin Velankar for their guidance and valuable feedback at different stages of my research work. I would also like to thank Prof. Jianzhong Wu and Dr. Shuangliang Zhao (UC Riverside) for great collaboration and valuable discussion.

To my wonderful labmates, classmates, colleagues, and friends, I deeply thank your great friendship and support throughout these years. I would like to express my sincere gratitude to everyone whom I have come in contact with during my PhD study for being part of my PhD experience.

Last but not the least; I would like to thank my family for their love, patience, and support throughout my seemingly endless school years.

1.0 INTRODUCTION

1.1 BACKGROUND ON DNA SEPARATION

1.1.1 Structure of DNA

DNA, or deoxyribonucleic acid, is a highly charged polyelectrolyte made up of a long chain of monomers, called nucleotides. The backbone of a DNA contains of four different types of nucleotides. Each nucleotide contains a phosphate group, a five-carbon sugar, and a heterocyclic nitrogenous base. The phosphate group is linked to the 5′ carbon of the sugar and the nitrogenous base is attached to the sugar's 1′ carbon. Different nucleotides are distinguished by their nitrogenous bases. Four different bases are present in DNA: adenine (A), thymine (T), cytosine (C), and guanine (G). The nucleotides are linked together via an ester bond between the phosphate group attached to the 5′ carbon of the sugar and the hydroxyl group attached to the 3′ carbon of the sugar of the next nucleotide to form a long chain. Two strands of these long chains can interact through hydrogen bonds by pairing A+T and C+G, respectively. The particular order of the bases along the sugar-phosphate backbone is called DNA sequence. The exact genetic information coded in the sequence is used to construct other parts of the cell, RNAs and proteins, via transcription and translation respectively. Determining the DNA sequence is therefore the key to understand fundamental biological processes as well as applications such as diagnostics, forensics and personal medicine designing.

1.1.2 Significance of DNA separation

DNA separation is one of the most widely used analytical methods in molecular biology and biochemistry, and it is a core method for genomic analysis. Many research, health care, and forensic applications rely on DNA separation. Measurement of the length distribution of DNA molecules in a heterogeneous solution is required in many biological assays. Analysis of a DNA fragment based on the respective size can provide information about the sequence within the fragment, or the DNA from which the fragment was derived, from which major properties of genes can be obtained. Therefore, separation of DNA and other biomolecules on basis of size is the most important tool in genetics and several applications are undoubtedly related to improvements in DNA separation. These include DNA sequencing, genome mapping, development of biotechnology or diagnosis of genetic diseases, and even broader applications in genetic fingerprinting or DNA profiling. DNA separation enabled the completion of the Human Genome Project, which aimed at the deciphering of the gene sequence buried in a DNA molecule and was a milestone towards the understanding of life, with new insights into the properties and functions of genes. Even though a finished version of the human genome sequence is now available, the ability to sequence complex genomes, including the human genome and other complete DNA sequences of many animal, plant, and microbial species, remains critically important for researchers in the biological sciences. Continued human genomic sequence determination is critical for the promise of medical care tailored to an individual’s unique genetic identity, because understanding the pathways and effects genetic irregularities have on abnormalities results in detection and actual solutions to diseases and disorders affecting humans worldwide. A challenge to realizing the true benefits of genomic analysis is that faster, less expensive and highly reliable sequencing methods must be developed and incorporated into routine detection methods, which will certainly benefit from the advances in DNA separation techniques.

1.1.3 DNA separation techniques

1.1.3.1 Slab gel electrophoresis

Gel electrophoresis is the most widely used method for DNA separation. Electrophoresis refers to the motion of charged analytes under the action of an external electric field. In electrophoresis, separations of analytes are typically based upon the differential migration of analytes in the presence of an applied electric field, which results from differences in the effective charge-to-size ratios of analytes. The separation of DNA molecules poses a challenge to free-solution electrophoretic techniques, because the charge-to-size ratio is similar for all DNA strands more than a few nucleotides in length.[1-3] The mobility is therefore size-independent in free-solution. The successful application of electrophoresis for DNA separation relied on the development of media such as sieving gels. The gel, usually polyacrylamide or agarose, is essential to the separation because it serves as a sieving matrix that affects the overall mobility of the DNA strand through steric interactions, with smaller strands moving through the gel faster than larger ones.[4-6] Polyacrylamide is a cross-linked polymer of acrylamide. The pore size of polyacrylamide gel is determined by the concentration of acrylamide used. Polyacrylamide gels are often used for high-resolution separations of smaller DNA fragments[7, 8] (less than 500 nucleotides or bp). Agarose is a marine polysaccharide, which forms a thermo-reversible gel.

Agarose gels are cross-linked by hydrogen bonds and, can form larger pores, which makes then suitable for the separation of larger DNA fragments in range from 100bp to several kilo bases.[9, 10] In a typical gel electrophoresis, DNA migrates through a gel with the application of a low electric field on the order of 1-10 V/cm to avoid generating excessive heat during a run. This often results in an upper limit for the efficient use of the technique.

1.1.3.2 Pulse field gel electrophoresis

The separation of large molecules (> 30 kilo base pairs) fails using conventional gel electrophoresis. Under a constant electric field, large molecules tend to orient their leading monomers in the direction of the field, leading to the mobility saturating to a size-independent value. However, the separation of large DNA molecules can still be achieved in gel electrophoresis when pulsed-field is applied.[11-18] It was found that DNA molecules demonstrate both size-dependent and size-independent velocity when subjected to field orientation changes. DNA molecules align from random conformation to the field direction in a size dependent way as a new field appears. When the steady state is reached, size-dependent velocity is no longer valid, and is replaced by the size-independent velocity. Therefore, for a given pulse frequency, longer fragments can not reach the steady state before pulse switching, while the shorter ones could migrate with steady state velocity, resulting in the larger ones lagging behind of the smaller ones. Pulsed field gel electrophoresis is a powerful tool that could separate DNA fragments from tens of kilo bases to few mega bases. While this extends the useful range of sizes, pulsed field gel electrophoresis remains a time consuming technique, as the separation of one chromosomal DNA for example can require up to several days.

1.1.3.3 Capillary electrophoresis

Capillary electrophoresis (CE) is an analytical technique that attracted much attention for its efficiency and high resolution.[19-23] The separation occurs in a narrow capillary tube with an inner diameter between 25-100 μm and a total length of about several centimeters. To prevent problems such as clogging or gel breakage, the separation matrices used in CE are usually more fluid than gels. Entangled polymer solutions are the most widely and successfully used ones.[24-26]

CE is very useful and efficient in operating fast separations with higher output than conventional gel electrophoresis. The high surface to volume ratio of the capillary could reduce Joule heating, which makes it possible to use high electric fields (normally 200-300 V/cm in CE, and less than 50 V/cm in conventional gel electrophoresis) leading to improved output and resolution. CE devices also introduced a high level of automation;[27] capillary-array automated sequencers[28, 29] allow separations at least one order of magnitude faster than slab-gel electrophoresis. The development of these types of automated devices enabled the completion of the human genome project earlier than expected.

In CE, the magnitude and direction of the electroosmotic flow, i.e., the fluid motion generated by the mobile counterions close to the charged surface of the capillary walls, is very important for optimization of peak resolution and analysis time. [30] It is difficult to achieve a well-resolved CE separation when the speed of electro-osmosis markedly exceeds that of analyte migration, due to the dominating nonselective transport. Coating the surface with polymers or silanization of surface silanol groups may reduce the effects of the electro-osmotic flow.[31-33] Similar to gel electrophoresis, there exists a critical size above which DNA molecules cannot be separated using entangled polymers in capillaries. However, the loss of resolution is attributed to hydrodynamic instabilities rather than chain orientation.[34, 35]

1.1.3.4 Micropost arrays

Inspired by the original idea of Volkmuth and Austin,[36] Doyle et al. and Kaji et al. designed a well-defined regular array of microposts,[37-42] with a diameter of 1μm. Experimental results and theoretical investigations of the mobility and the diffusivity of DNA based on a model of single-post collisions and random translation between the collisions, indicate that the resolution is independent of the electric field magnitude. In contrast to gel electrophoresis, separations of long DNA (50-150 kb) within a few minutes were reported.

1.1.3.5 Entropic traps

Han et al.[43-45] developed an entropic-based system for DNA separation with a nanochannel consisting of alternating thick and thin regions. DNA molecules moving along the channel in an applied electric field get trapped in the thick regions with an escape rate that is related to their size. The longer molecules have a greater surface contact area with the boundary and therefore have a higher probability of escaping into the thin regions than the shorter chains, leading to size-dependent separation. Another entropy-based system is a chip[46, 47] containing two different regions—a plane region and a region containing a dense array of nanopillars. The entropy of a DNA molecule is lower in the pillared region, where it adopts fewer configurations than in the plane region. With the application of an electric field, DNA molecules, originally placed at the plane–pillared region interface, pass through the pillared region. Smaller molecules enter the pillared region entirely, whereas larger molecules entered only partially. The part of the longer molecule trapped by the pillared region experiences an entropic force. When the electric field is turned off, the larger molecules tend to recoil back and enter into pillar-free region where the entropy is maximized. Smaller molecules that are completely present in either of the two regions do not experience any force owing to their uniform entropies.

1.1.3.6 Self-assembly of supermagnetic beads

Doyle et al.[48] took advantage of the self-assembly properties of supermagnetic beads to create a quasi-two-dimensional array of columns comparable to post arrays in a thin region between two plates without the use of sophisticated lithographic techniques. The spacing between the columns or the pore size may be tuned by varying the particle concentration and the distance between the plates. Such a device has the ability to vary the pore size (from 1 to 100 mm) with time that helps in the separation of DNA molecules of a wide size range. Based on the same concept, various ordered sieving structures have been proposed for DNA separation.[49-52] The main idea is to induce the self-assembly of colloidal particles, to construct a well ordered nanostructure that can be used to sort DNA molecules. While earlier devices focused on the void spaces between the particles as a sieving matrix in the microfluidic, the inverse structures, consisting of well-ordered spherical cavities, connected by narrow pores, are also currently used for DNA separations, as well as the study of single-molecule behavior in confining geometries.

1.1.3.7 Nanopores

Nanopore analysis is an emerging technique that uses a voltage to drive molecules through a nanoscale pore in a membrane between two electrolytes, and then monitors change of the electrolytic current through the nanopore as single molecules translocate through it. For example, a nanopore formed from staphylococcal a-hemolysin reconstituted in a lipid membrane has been used like a molecular-scale Coulter counter.[53] When a voltage is applied across the membrane, DNA in electrolyte passes through an a-hemolysin pore, temporarily blocking the electrolytic current through the pore. The magnitude and duration of the blocking transient provides a signal that has been used to discriminate between individual DNA hairpins differing by a single base pair. Nanopores can be a biological protein pore [54-56] or a pore in a solid-state membrane.[57-60] Biological nanopores have advantages such as, the atomic precision in assembly; almost perfect repeatability of nanopore structure; and the ability to use genetic techniques to tailor the physical and chemical properties. Solid-state nanopores are becoming highly versatile alternative to biological nanopores due to several advantages such as tunable diameter and shape with subnanometre precision, the ability to fabricate high-density arrays of nanopores, superior mechanical, chemical and thermal properties, and the possibility of integrating with electronic or optical readout techniques. The major challenges in the field are to reduce the speed at which the DNA molecule translocates through the nanopore (so that the bases can be reliably identified) and to improve the sensitivity, which will require new sensing methodology and devices.[61]

1.2 SEPARATION OF CELLS: BACKGOUND AND SIGNIFICANCE

Separation of biological targets, such as cells, proteins and peptides, from other sample components is an important process for sample preparations, which are the foundations for medical diagnostics, therapeutics, and environmental monitoring. It is essentially useful to separate the desired rare cells from a number of cells quickly and accurately.[62-67] For example, circulating tumor cells (CTCs) in cancer patients are strong predictors of the spread of cancer from primary to metastatic disease.[68-71] The level of CTCs detected in body fluids such as whole blood and urine yields prognostic information and might help tailor systemic therapies to the individual needs of cancer patients. However, the concentration of cancer cells in a blood sample is very low (100 cells/mL normally) compared to other blood cell types.[72, 73] As a result, technologies capable of rapidly isolating rare desired targets from a heterogeneous population are highly demanded.

Several techniques have been reported for the effective isolation and purification of target cells. Among them, the immuno-based techniques such as fluorescence-activated sorting[74-77] and magnetic-activated sorting[76, 78-82] have been successfully applied in practical applications, for example, isolation of target cancer cells from the clinical samples. Based on the specific affinity between the surface antigens of cancer cells and the fluorescent dye-labeled antibodies or immunologically labeled magnetic beads, target cells can be indentified and then sorted for further analysis. Another filtration-based method has been demonstrated to successfully separate circulating tumor cells from a peripheral blood sample by using a membrane filter.[83, 84] However, large and expensive equipment such as centrifuges and shakers, as well as well-trained personnel is required. Moreover, the lengthy diagnosis protocol is relatively costly and time-consuming.

The microfluidic-based sorting technique improves the process by miniaturizing amount of equipment, reducing costs and increasing flexibility.[85-89] Despite their success in manipulating microliter amounts of simple liquids, they have thus far shown limited capability to deal with large volumes (milliliters) of complex samples.[90, 91] Additionally, false results caused by the non-specific interactions between the targets and the surfaces encountered in the separation process are unavoidable in practical applications regardless of the differences in varied techniques. Therefore, there has been steadily growing interest in developing new strategies for the isolation of rare targets from a heterogeneous mixture with a higher sensitivity and efficiency.

1.3 OVERVIEW OF OUR RESEARCH

Developing alternative separation technologies for DNA molecules of various lengths have attracted considerable attention as they reduce the cost of genome sequencing, and allow separation of intact chromosomes, construction of long-range gene maps, cloning of large DNA fragments, and discovery of chromosome-length polymorphisms. In the first part of my dissertation, we have developed novel DNA separation technologies that are fundamentally different from the conventional electrophoresis-based ones. Separation of DNA was based on first tethering DNA fragments onto a solid surface through precise end-hybridization and then sequentially pulling the DNA off the surface using an electric field. The anchor is such designed that the critical force to detach a DNA fragment is independent of the chain length. Because the electrical force applied to each DNA fragment is proportional to its net charge, a gradual increase of the electric field leads to a size-based detachment of the DNA strands-longer DNA fragments first departing the surface followed by the shorter ones.

Based on this concept, we first immobilized long double-stranded (ds) DNA molecules on a glass slide through short DNA anchors attached to its surface. We then put the sample between two conducting glasses in a chamber filled with a buffer solution. Application of a DC electric field stretches out the long dsDNA molecules, resulting in forces that break the hydrogen bonds linking them with the shorter DNA anchors connected to the substrate. The DNA molecules were covalently labeled with fluorophores for the detection of detachment of the DNA molecules from the surface. We have demonstrated efficient separation of lambda-DNA (a standard length of viral DNA containing 48,502 base pairs) from human DNA comprising about 100,000 base pairs (Chapter 2). This simple and highly efficient separation technology can be implemented with a simple DC electrical field, does not require separation matrices such as gels or polymer solutions, and in principle has no upper limit on the length of the DNA that can be efficiently separated.

Separation of short DNA fragments, which is required for DNA sequencing, by the above experimental setup for long DNA separation is challenging because an extremely large electric field is needed to load the short DNA fragments with a large enough stretching force that can pull them off the surface. Such large electric field requires very high electric potential, which may cause various problems such as Joule heating and side electrochemical reactions in the buffer solution. In Chapter 3, we developed an integrated microfluidic platform for separation of short DNA fragments. We applied geometric variation to the microfluidic channel to generate high electric fields with relatively low electric potential and employed a low conductivity buffer to further reduce the electric current. We were able to use the strong electric field to pull short single-stranded DNA (ssDNA) fragments off the surface with negligible Joule heating in the microchannel. Efficient separation of single-stranded DNA at a 10-nucleotide resolution was demonstrated. Theoretical analysis indicates that the separation resolution is limited by the fluctuation forces on tethered DNA chains.

In Chapter 4, we developed a second approach for separation of short ssDNA fragments by taking the advantage of the strong yet evolving non-uniform electric field near the Au surface in contact with a buffer solution which is gradually diluted by deionized water. We showed that by tethering the ssDNA to an Au electrode and applying a relatively low electrode potential on the Au electrode, ssDNA strands of different lengths can be separated by gradually diluting the buffer solution in contact with the Au electrode. The high electric field strength inside the electrical double layer at the gold/electrolyte interface allows us to pull short ssDNA strands off the surface with a very low electrode potential. Electrochemical reactions are avoided by maintaining the low electrode potential within the ideally polarizable region. Tuning the ion concentration of the electrolyte solution allows regulation of the non-uniform electric field. By gradually decreasing the ion concentration, longer ssDNA strands are detached first and then followed by the shorter ones. A numerical analysis based on a simple electric double layer model provides semi-quantitative explanations of the experimental results.

In the second part of this dissertation (Chapter 5), we presented a multistage magnetic separation scheme that is able to effectively circumvent the problem caused by the non-specific interactions by introducing multiple capture-and-release cycles to the magnetic separation process. We have demonstrated a multistage magnetic separation process that is able to separate PNIPAM-functionalized PS microspheres from bare PS microspheres by using PNIPAM-functionalized MNPs. The reversible hydrophilic-to-hydrophobic transition of PNIPAM molecules enables us to manipulate the hydrophobic interactions between the MNPs and the microspheres upon cycling the temperature, and to separate the target microspheres from non-target microspheres in multiple stages through capture-and-release cycles. The overall enrichment factor is observed to significantly increase with the number of separation stages, and reaches as high as 1.87×10^{5} after 5 stages.

2.0 SEPARATION OF LONG DNA MOLECULES THROUGH CLEAVAGE OF HYDROGEN BONDS UNDER A STRETCHING FORCE

We develop a novel technology of separating long DNA molecules in different lengths by breaking hydrogen bonds that tether the DNA molecules to a substrate. The hydrogen bonds are broken by stretching the DNA molecules in an electric field, which produces forces proportional to the length of the DNA. This separation technology can be implemented with a simple DC electrical field, does not require separation matrices such as gels or polymer solutions, and has no upper limit on the length of the DNA that can be efficiently separated. Efficient separation of Lambda DNA (48,502 bp) from human genomic DNA (> 100 kbp) using this technology is demonstrated.

2.1 INTRODUCTION

DNA separation by length is the foundation for DNA sequencing, manipulation, analysis, and cloning in molecular biology. Classical gel and capillary electrophoresis—the current core technologies for DNA separation—have an upper limit of about 40 kbp (kilobase pair) on the length of the DNA that it can efficiently separate.[92] Separation technologies for long DNA molecules are demanded, as they reduce the cost of genome sequencing[93] and allow separation of intact chromosomes,[94] construction of long-range gene maps,[95] cloning of large DNA fragments,[96] and discovery of chromosome-length polymorphisms.[97] Pulsed field gel electrophoresis[98] (PFGE) and pulsed field capillary gel electrophoresis[99] (PFCGE) have raised the upper length limit of DNA separation in agarose from 30 to 50 kbp to over 10 Mbp (megabase pair). Although PFGE and PFCGE have profoundly altered the study of genes and genomes as both preparative and analytical tools, they both have intrinsic upper limits on the length of the DNA that they can efficiently separate. In addition, they are time consuming and cumbersome, and they require complex methods to recover the separated DNA from the gel. Therefore, there has been considerable interest in developing alternative technologies for long DNA separation, among which entropic trap arrays,[44] diffusion sorting arrays,[40] and transports of DNA in microfluidic and nanofluidic channels[100] have shown promising results. However, significant improvements are still needed to incorporate these technologies into established bioanalysis protocols for wide applications.

Here, we develop a technology for separating long DNA molecules by cleaving hydrogen bonds that tether one end of the long DNA molecules to a short DNA probe immobilized on a surface. The hydrogen bonds are cleaved by stretching the DNA in an electric field, which produces forces proportional to the length of the DNA—longer DNA molecules possess more negative charges at a physiological *p*H and thus are loaded with greater forces than shorter ones. Therefore, the longer DNA molecules are unzipped from the probe and depart the surface earlier than the shorter ones when the strength of the electric field is gradually increased. This separation technology in principle has no upper limit on the length of the DNA that can be efficiently separated.

We demonstrate efficient separation of lambda double-stranded (ds) DNA (48 502 bp) from human genomic ds-DNA (90% of the sample is greater than 100 kbp in size) based on length difference. Lambda DNA and human genomic DNA are covalently labeled with fluorophores Alexa 488 and Alexa 568, respectively, before they are mixed and used as our DNA mixture sample. The separation results are monitored using the fluorescence intensities detected from the DNA molecules.

2.2 STATISTICAL MECHANICS MODEL OF UNZIPPING DOUBLE STRANDED DNA

Similar to the bulk thermally driven melting transition of dsDNA, the unzipping of dsDNA under a stretching force can be described at varying levels of details by a number of models, all of which are expected to give the same universal behavior on long enough length scales. One popular choice is an Ising-like description,[101] in which a base pair is taken to be in one of two discrete states-open or closed. By convention, the free energy of an unconstrained base pair in the open state is set to zero. The Hamiltonian of a semi-infinite strand can be written as a sum of energies associated with successive paired and unpaired regions. In the continuum limit, the simplest such description of a dsDNA of finite length *N* has the Hamiltonian:

$$\mathrm{H}_C = \int_0^N dn \left\{ \frac{k_B T d}{4ab} \left(\frac{dR}{dn} \right)^2 + V_n \left[R(n) \right] \right\} \tag{1}$$

where $R(n)$ is the relative displacement of the two single strands at base pair n, d is the spatial dimension, a is the backbone length of a chemical monomer along a single strand, b is the Kuhn length of single-stranded DNA, $k_B = 1.38 \times 10^{-23}$ J/K is the Boltzmann constant, and T is the temperature at which the DNA is stretched. The first term describes the entropic elasticity of the single strands, and the second term accounts for the attractive interactions between the two single strands.

This model can be readily extended to include a force pulling apart the double-stranded molecule. A constant force acting at the end of the DNA to separate the two single strands contributes an energy that is linear in their separation. For the continuum model, one can add a term to the Hamiltonian of the form:

$$\mathrm{H}_{C,pull}(F) = -F \cdot r = \int_0^N dnF \cdot {dR}/{dn} \cdot \qquad (2)$$

When both strands of the DNA to be separated are linear and can be considered as a Gaussian chain.

By viewing the energy H_C and $\mathrm{H}_{C,pull}$ of the continuum model (Eqns. 1 and 2) as an imaginary time quantum mechanical action, the critical force (F_c) upon which the dsDNA unzips can be estimated by:

$$F_c = \frac{\sqrt{k_B T |g_0|}}{b} \qquad (3)$$

Here g_0 is the average binding energy per base pair of dsDNA, b is the Kuhn length of the single-stranded DNA. Schematic phase diagram in the temperature– pulling force (*T*-*F*) plane of a dsDNA molecule in three dimensions is shown in Figure 1. At large enough forces the dsDNA will unzip completely, whereas for very small forces at most a few bases will open. The phase diagram shows that these two regimes are separated by a sharp first-order phase transition. Below the critical force *Fc*, only a finite number of bases at the end of the double strand are pulled open; in the thermodynamic limit of an infinitely long DNA molecule, the pulling force thus has no effect on the fraction of open bases, which remains very small in physiological conditions. Above *Fc*, the entire molecule unzips, and the fraction of open bases jumps discontinuously to one.

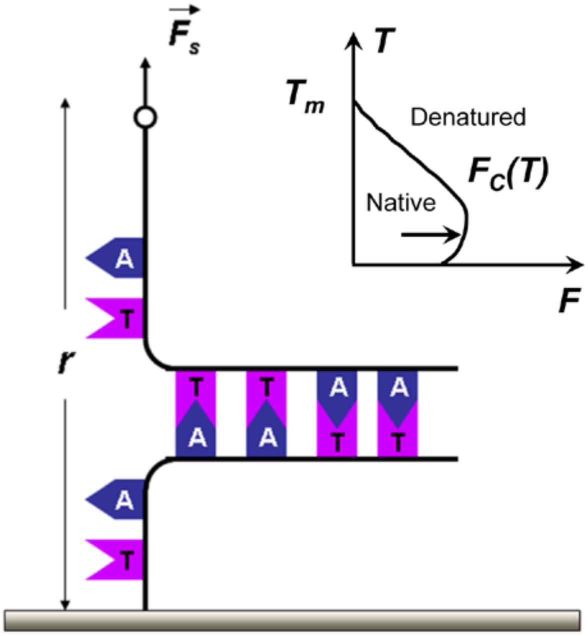

Figure 1. Schematic model of the DNA unzipping transition. One of the strands of the dsDNA molecule with a base sequence consisting of A and T bases is attached by its end to a solid surface, and the other strand is pulled away from the surface with a constant force F. As a result, the double strand partially denatures, separating m base pairs (m = 2 in the figure). The distance between the ends of the two single strands, or extension, is r. Inset is a schematic phase diagram[101] in the temperature (T)-pulling force (F) plane of a dsDNA molecule.

2.3 SEPARATION OF LAMBDA DOUBLE STRANDED DNA FROM HUMAN GENOMIC DOUBLE STRANDED DNA

We expect to separate lambda double-stranded (ds) DNA (48,502 bp) from human genomic ds-DNA (90% of the sample is greater than 100 kbp in size) based on length difference. Lambda

DNA and human genomic DNA are covalently labeled with fluorophores Alexa 488 and Alexa 568, respectively, before they are mixed and used as our DNA mixture sample. The separation results are monitored and reported using the fluorescence intensities detected from the DNA molecules.

Figure 2 schematically shows the separation process. It began by tethering the 3′ end of the lambda DNA and the human genomic DNA to the surface of a glass slide via hydrogen bonds between a series of thymine (T) bases of a poly-T oligonucleotide probe immobilized on the glass and a series of adenine (A) bases of a short poly-A tail added to the 3′ end of the long ds-DNA (Fig. 2a). The poly-T probe was a 3′-amine-modified 20-mer (5′-TTTTTTTTTTTTTTTTTTTT-NH2-3′) and was covalently immobilized to the amine-functionalized glass slide via glutaraldehyde. The poly-A tail consisting of 50-100 A bases was added to the 3′ end of the long ds-DNA molecules by a terminal transferase-catalyzed reaction. The poly-A tail of the long DNA molecules was then hybridized with the poly-T probe via a series of hydrogen bonds (N-H··· O and N··· H-N) between the A-T base pairs (Figure 2b).

The glass slide with immobilized long DNA molecules was then loaded into a chamber made by sandwiching a polydimethylsiloxane (PDMS) membrane between two indium tin oxide (ITO)-coated glass slides (Figure 3). The ITO-coated glass slides provide a transparent window for observing the sample inside as well as a conducting layer that can be connected to a dc power source to form an electric field across the chamber. The distance (*d*) between the two ITO conducting layers at the top and bottom of the chamber was 5 mm. After the chamber was filled with a trisborate ethylenediamine tetra-acetic acid (TBE) buffer solution (*p*H 8.3), a dc voltage was applied across the chamber and was increased stepwise from 0 to 400 mV with an increment of 25 mV. The buffer solution was collected and replaced with a fresh buffer after each increment of the dc voltage. The inside glass slide with immobilized DNA was observed under a fluorescence microscope after each time the buffer solution was collected.

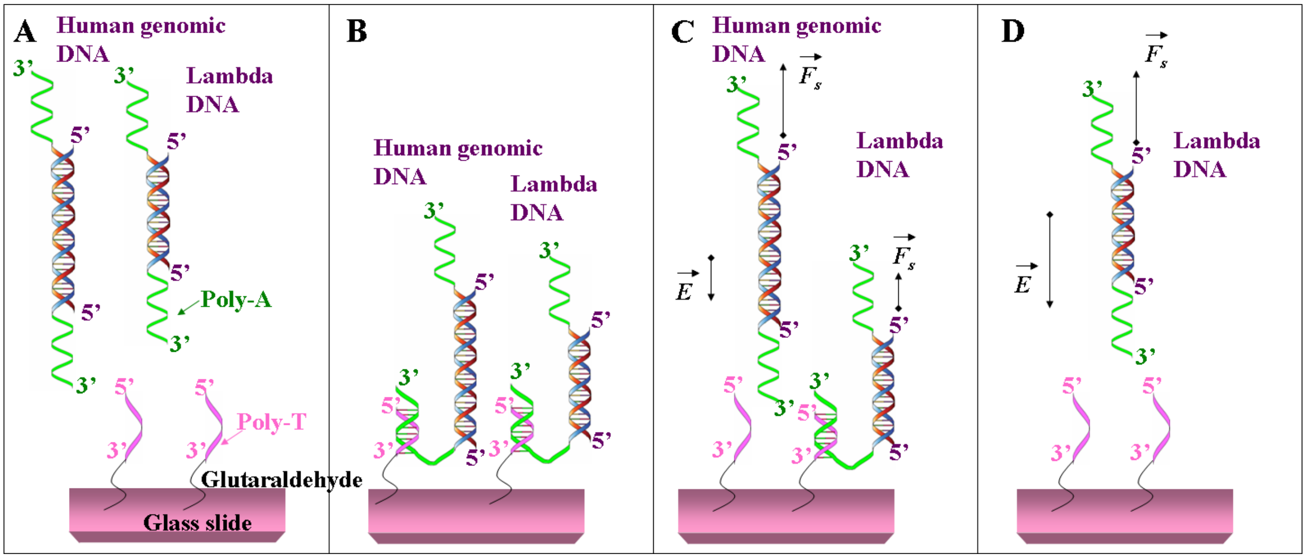

Figure 2. Schematic process flow for separating lambda DNA from human genomic DNA by length. (a) A poly-A tail is added to the 3' ends of the DNA molecules using a terminal transferase, and a poly-T probe is immobilized on the surface of a glass slide by covalently linking the amine-modified 3' end. (b) The DNA molecules with the poly-A tail are hybridized with the poly-T probe, and therefore are tethered to the substrate via a series of hydrogen bonds between the A-T base pair. (c) When a DC electric field (*E*) is applied, the DNA molecules are loaded with a stretching force (*F*), which is proportional to the length (the number of base pairs) of the DNA. When the force exceeds the strength of the hydrogen bonds between the A-T base pair, the base pairs start to dissociate, and the long DNA molecules are detached from the substrate. Because the human genomic DNA is longer than the lambda DNA and thus possesses more negative charges, they are loaded with greater stretching force and detached earlier than the lambda DNA as the strength of is gradually increased. (d) After the strength of further increases, the lambda DNA is also detached from the substrate, but separately from the human genomic DNA.

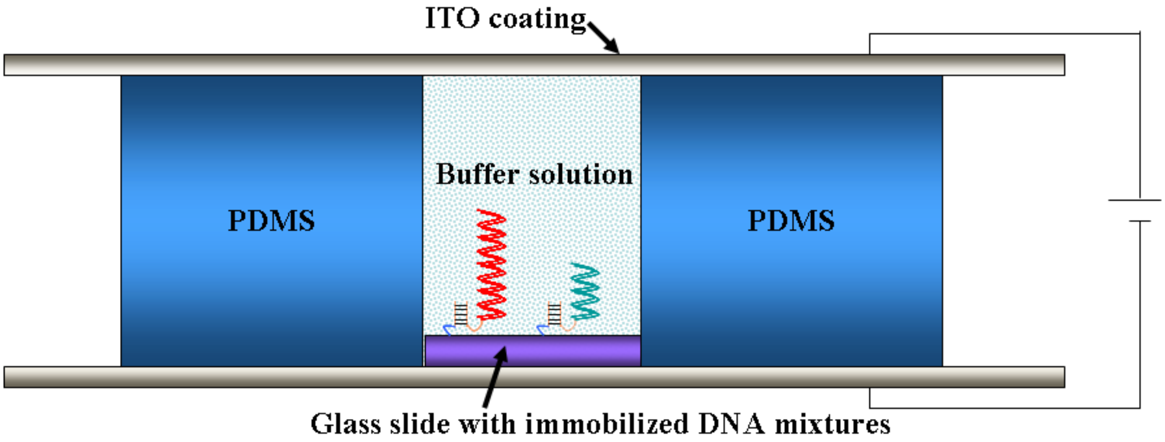

Figure 3. Schematic experimental setup for long DNA separation. A chamber is formed by sandwiching a PDMS membrane between two ITO-coated glass slides. The ITO coating provides a conducting layer that can be connected to a dc power source to apply an electric field across the chamber.

Figure 4 shows the fluorescence images of the glass slide with immobilized DNA molecules taken after applying dc voltages varying from 0 to 400 mV. The fluorescence intensities are plotted as a function of the DC voltage in Figure 5a. It is observed that the fluorescence intensity detected from the fluorophore-labeled human genomic DNA starts to decrease significantly when the applied DC voltage is 25 mV, and reaches nearly a constant value when the voltage exceeds 100 mV. In contrast, the fluorescence intensity detected from the lambda DNA stays almost constant until the voltage is increased to 250 mV, after which it starts to decrease dramatically and reaches a nearly constant value as the voltage is greater than 250 mV. Figure 5b plots the fluorescence intensities decrease corresponding to the amount of DNA detached from the substrate when the DC voltage is increased stepwise. It is obvious that the lambda DNA is separated from the human genomic DNA.

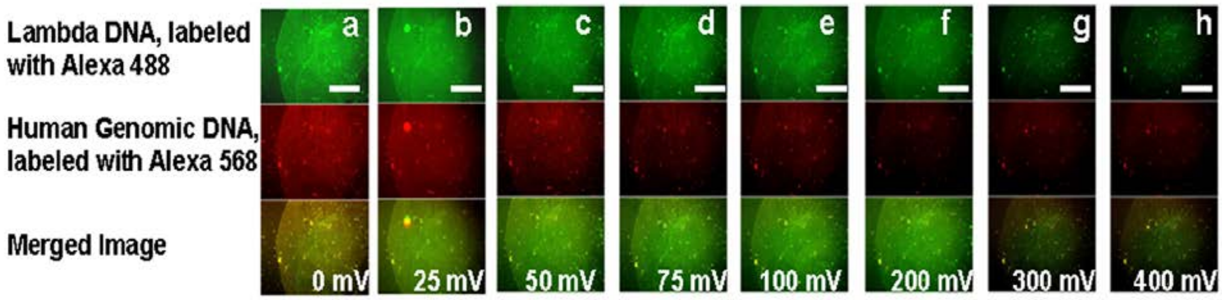

Figure 4. Fluorescence images of the glass slide with immobilized DNA mixtures consisting of lambda DNA (labeled with fluorophore Alexa 488) and human genomic DNA (labeled with fluorophore Alexa 568) when a stepwise increasing DC voltage is applied. The images are taken after (a) 0, (b) 25, (c) 50, (d) 75, (e) 100, (f) 200, (g) 300, and (h) 400 mV DC voltage is applied, respectively. The scale bars are 300 μm.

The long DNA molecules are polyanions at *p*H 8.3 in the TBE buffer solution. When the DC voltage (*V*) is applied with an electric field ($\vec{E}$) facing the glass surface, the DNA molecule is loaded with an electrostatic force ($\vec{F}_s$) that stretches it out of the glass surface (Fig. 2c), which is proportional to the amount of charge that the DNA molecule possesses and to the applied dc voltage. Following an earlier DNA electrophoretic measurement,[102] we estimate that the stretching force is given by $\vec{F}_s = 0.1\mathrm{eN}\vec{E}$, where 0.1e is the effective charge per base pair of the DNA in the TBE buffer and N is the total number of base pairs. When the stretching force exceeds the strength of the hydrogen bonds (N—H·O and N··· H–N) between the A-T base pairs, the poly-A tail of the long DNA molecule unzips from the poly-T probe and the long DNA molecule departs the surface (Fig. 2c). Because the unzipping of the poly-T from the poly-A follows a first-order phase transition,[103] dissociation of the base pairs takes place in an avalanche manner. As a result, the stretching force that is needed to break the hydrogen bonds between a series of A-T base pairs is mainly determined by the binding strength of one A-T base pair rather than the number of A-T base pairs tethering the long DNA to the poly-T probe. We estimate that at 296K, the A-T base pairing energy (g_0) is -0.705 kcal/mol.[104]

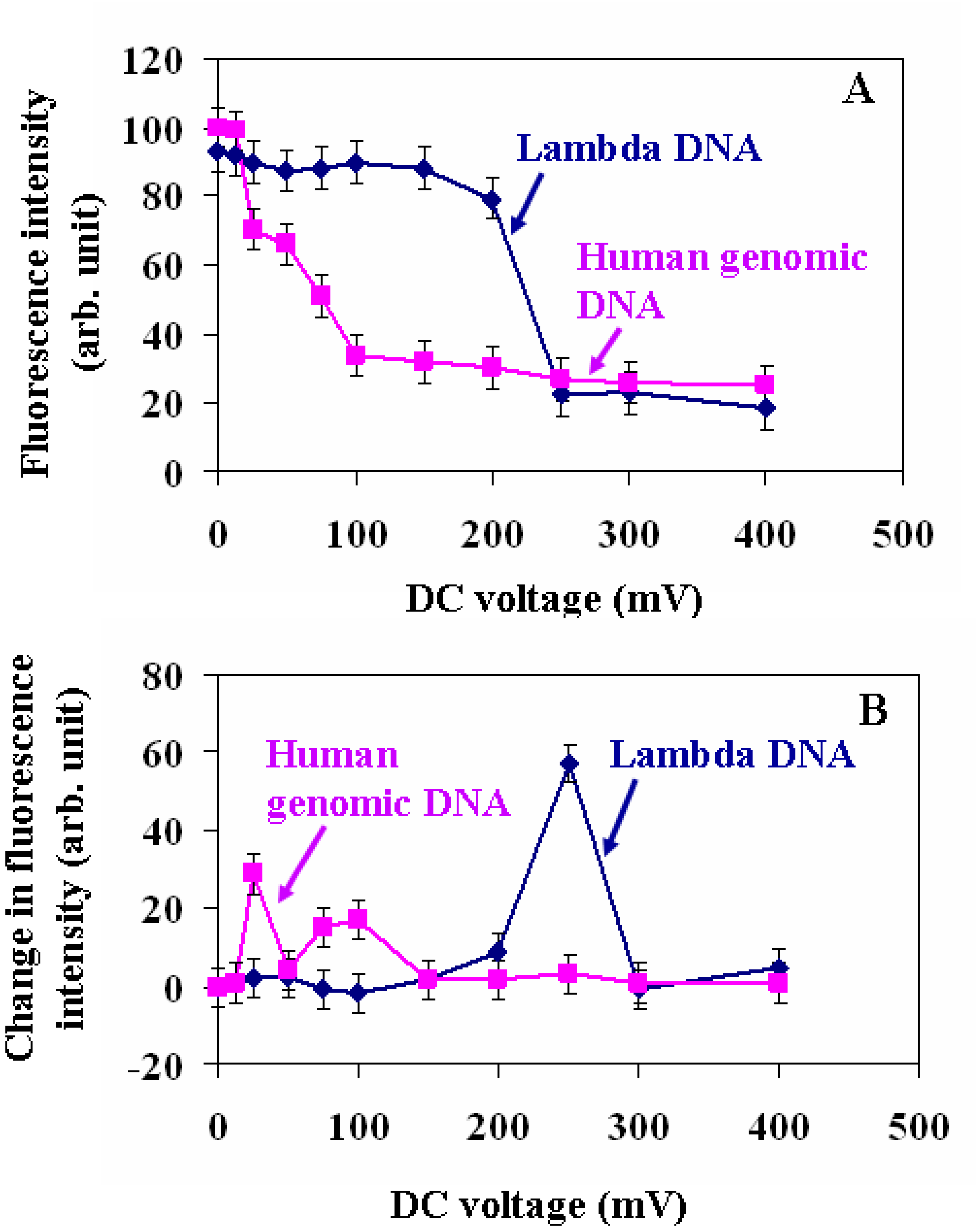

Figure 5. (a) Fluorescence intensities detected from the fluorophore-labeled lambda DNA and human genomic DNA as a function of the applied DC voltage. (b) The decrease in the fluorescence intensities corresponding to the amount of DNA detached from the substrate when the DC voltage is increased stepwise.

While the stretching force that is needed to detach the long DNA molecules from the surface is independent of the DNA length, longer DNA molecules are loaded with greater stretching forces than shorter ones under the same electric field. Therefore, when the strength of the electric field gradually increases, the stretching force loaded to the longer DNA molecule induces the dissociation of the A-T base pairs first and the longer DNA molecules are detached from the substrate earlier than the shorter ones (Figure. 2c). Thus, by gradually increasing the dc voltage across the chamber, DNA molecules of different lengths can be separated, with longer ones detached from the substrate first.

Calculation of the stretching force loaded to the lambda DNA at 250 mV gives a critical value of 0.039 pN for inducing the disscociation of the A-T base pair. This value is comparable to the mechanical unzipping force of $\vec{F}_c = \sqrt{k_B T |g_0|} / b$ = 0.045 pN predicted on the basis of a Gaussian-chain model for long DNA,[101] where k_B = 1.38×10^{-23} J/K is the Boltzmann constant, T = 296K is the temperature at which the DNA is stretched, and b = 100 nm is the Kuhn length for ds-DNA.

2.4 CONCULSIONS

The above result demonstrates the potential of this technology for efficient separation of long DNA molecules, although further investigation is needed to quantify the separation resolution of this technology. Because the proportionality between the stretching force and the length of the DNA holds regardless of the DNA length, this technology in principle has no upper limit on the size of the DNA that can be efficiently separated. The separation process does not require separation matrices such as gels or polymer solutions, complex lithography techniques, or power supplies to generate a pulsed field. The recovery of the DNA after separation is straightforward. There is no apparent technical barrier either to scale up the device for batch operation or to shrink it down to micrometer size for integration with lab-on-a-chip systems. The simplicity of this technology will greatly facilitate its incorporation with established bio-analysis protocols. In addition, such a system may provide an effective experimental approach for investigating the dynamic strength of hydrogen bonds between DNA strands.

3.0 SEPARATION OF SINGLE-STRANDED DNA FRAGMENTS AT A 10-NUCLEOTIDE RESOLUTION BY STRETCHING IN MICROFLUIDIC CHANNELS

We have developed a novel DNA separation method by tethering DNA chains to a solid surface and then stretching the DNA chains with an electric field. The anchor is such designed that the critical force to detach a DNA chain is independent of its size. Because the stretching force is proportional to the DNA net charge, a gradual increase of the electric field leads to size-based removal of the DNA strands from the surface and thus DNA separation. Here we show that this method, originally proposed for separation of long double-stranded DNA chains (>10 000 base pairs), is also applicable to single stranded (ss) DNA fragments with less than 100 nucleotides (nt). Theoretical analysis indicates that the separation resolution is limited by the fluctuation forces on tethered DNA chains. By employing a microfluidic platform with narrow channels filled with a buffer of low ionic conductivity, we are able to apply a strong electric field to the DNA fragments with negligible Joule heating. Upon stepwise increments of the electric field, we demonstrate efficient separation of short ssDNA fragments at a 10-nt resolution.

3.1 INTRODUCTION

DNA separation by size is the foundation of biotechnology for DNA sequencing, manipulation, and bioinformatics analysis. Motivated by the broad applications of DNA separation, we have been developing a novel DNA separation method that is fundamentally different from classical gel and capillary electrophoresis. Our method is based on first tethering DNA fragments onto a solid surface through precise end-hybridization and then sequentially pulling the DNA off the surface using an electric field.[105] The anchor is such designed that the critical force to detach a DNA fragment is independent of the chain length. Because the electrical force applied to each DNA fragment is proportional to its net charge, a gradual increase of the electric field leads to a size-based selection of the DNA strands—longer DNA fragments first departing the surface followed by the shorter ones. This separation strategy may provide a convenient, low-cost, and high-speed alternative to existing methods for DNA separation.[40, 41, 44, 48, 99, 106-110] Because the new method does not require separation matrices such as gel or polymer solutions, and in principle there is no upper limit on the size of DNA fragments that can be efficiently separated. Efficient separation of lambda DNA (48,502 base pairs) from human genomic DNA (> 100,000 base pairs) has been demonstrated using this method.[105] However, it remains unknown whether this method is applicable to separation of short DNA strands, e.g. with less than 100 nucleotides (nt), in which case, the solvent-induced fluctuation force on DNA fragments become significant in comparison with the incremental electric force and such fluctuation may severely compromise the separation efficiency. In addition, it is challenging to conduct experiments for separation of short DNA strands by employing the same experimental setup, e.g. a chamber made by sandwiching an insulating membrane between two conducting plates, which we have used for separation of the long DNA molecules. This is because a strong electric field (on the order of 10^5 V/m) is needed to load short DNA strands in order to pull them off the substrate. The large electric field may cause various technical problems such as Joule heating and side electrochemical reactions.

Here we show that by employing a microfluidic platform with narrow channels filled with a low conductivity buffer, we are able to use a strong electric field to pull short single-stranded DNA (ssDNA) fragments off the surface with negligible Joule heating. Efficient separation of single-stranded DNA at a 10-nucleotide resolution is demonstrated by first tethering the DNA fragments onto a solid surface through precise end-hybridization and then sequentially pulling the DNA off the surface using an electric field applied along a microfluidic channel. Theoretical analysis indicates that the separation resolution is limited by the fluctuation forces on tethered DNA chains, which agrees well with experimental results.

3.2 EXPERIMENTAL DESIGN

Figure 6 presents the schematic process for separating the short ssDNA stands by length in a microfluidic channel. First, ssDNA of different lengths are hybridized with the common biotinylated DNA probes (Fig. 6a). Then, the hybridized ssDNA-probe duplexes are introduced into the microchannel and are immobilized onto the streptavidin-coated bottom surface of the microchannel via strong biotin-streptavidin interaction (Fig. 6b). Upon application of a DC electric field (E) along the microchannel, each ssDNA strand is loaded with a stretching force with the strength proportional to its size. When the stretching force is sufficiently large, the ssDNA strands unzip from the probe and are sequentially detached from the surface (Figure 6c-6d). Because longer ssDNA fragments are detached earlier than the shorter ones, ssDNA strands of different lengths are thus separated.

Figure 7a presents the schematic top and side views of the microfluidic device employed in our experiments. The widths of the narrow and wide sections of the channel are 50 μm and

500 µm, respectively. The depth of the microchannel is around 35 µm. The total channel length is about 5 mm and the length of the middle narrow part is about 1 mm. A reservoir (~ 3 mm in diameter) is made at each end of the channel. The channel is filled with 20 mM histidine buffer, and two platinum electrodes are placed in the reservoirs, which connect the liquid buffer to a voltage source that applies a DC potential in a staircase waveform (step potential: 50 V, step period: 1 s, as shown in Figure 7b) along the microchannel. Figure 7c displays a representative electric field profile inside the microchannel (the potential drop along the entire channel is 100 V in this particular case), which is simulated by using a 2D finite element analysis software (COMSOL Multiphysics). With this microchannel configuration, a uniform electric field may be obtained in the middle region of the channel where the ssDNA fragments are stretched and imaged.

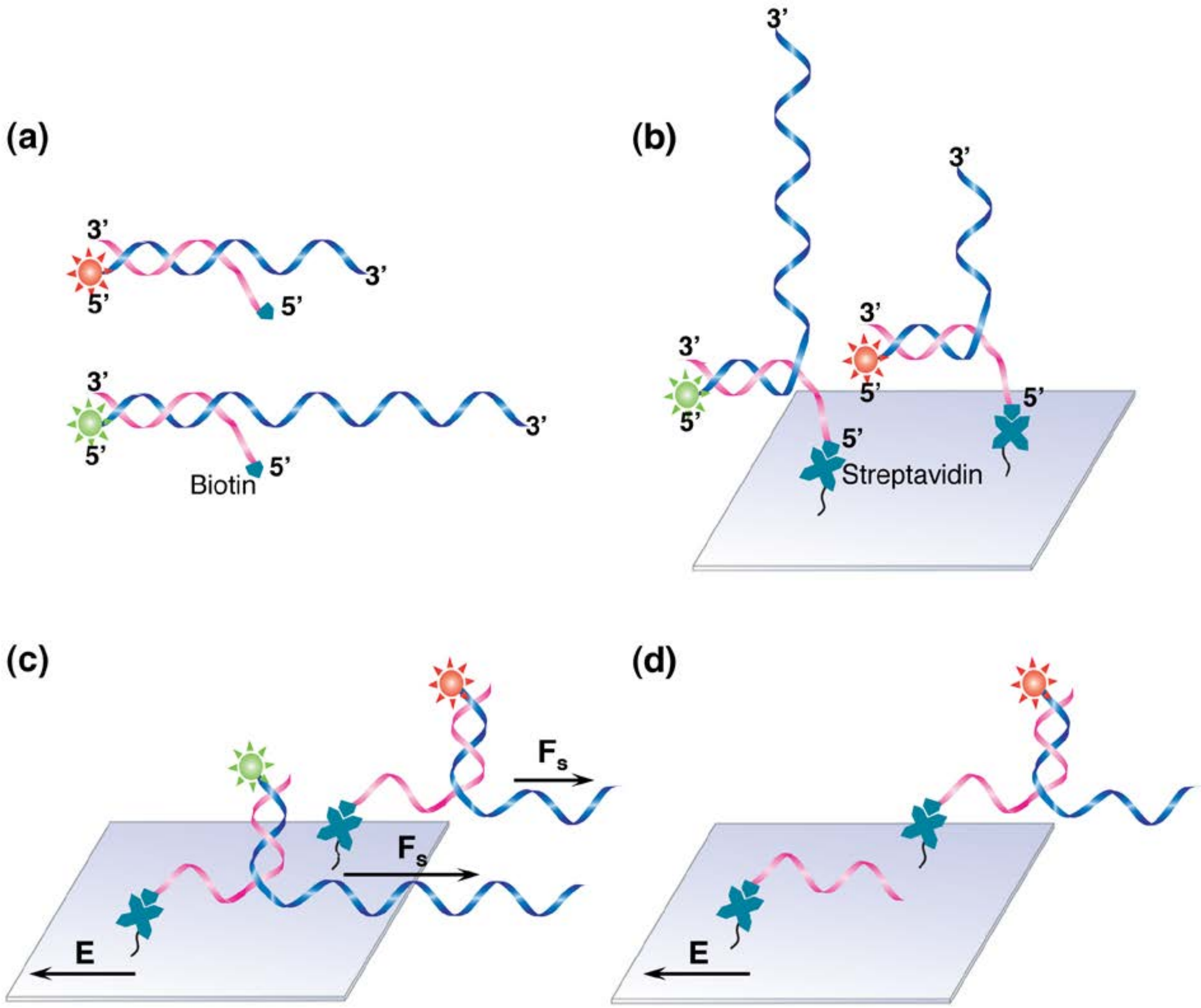

Figure 6. Schematic steps for separation of ssDNA. (a) ssDNA strands in varied lengths are hybridized with a common biotinylated probe. (b) The hybridized ssDNA-probe duplexes are immobilized onto the glass bottom surface of a microchannel via biotin-strepavidin interaction. (c) The DNA is stretched in a DC electric field (*E*). When the stretching force is large enough, the ssDNA strands unzip from the probe and are detached from the surface. Because the longer DNA is loaded with greater stretching force (F_s) than the shorter one at the same *E*, when *E* is gradually increased, the longer one is detached earlier than the shorter one. (d) The longer DNA is pulled off the surface and separated from the shorter one.

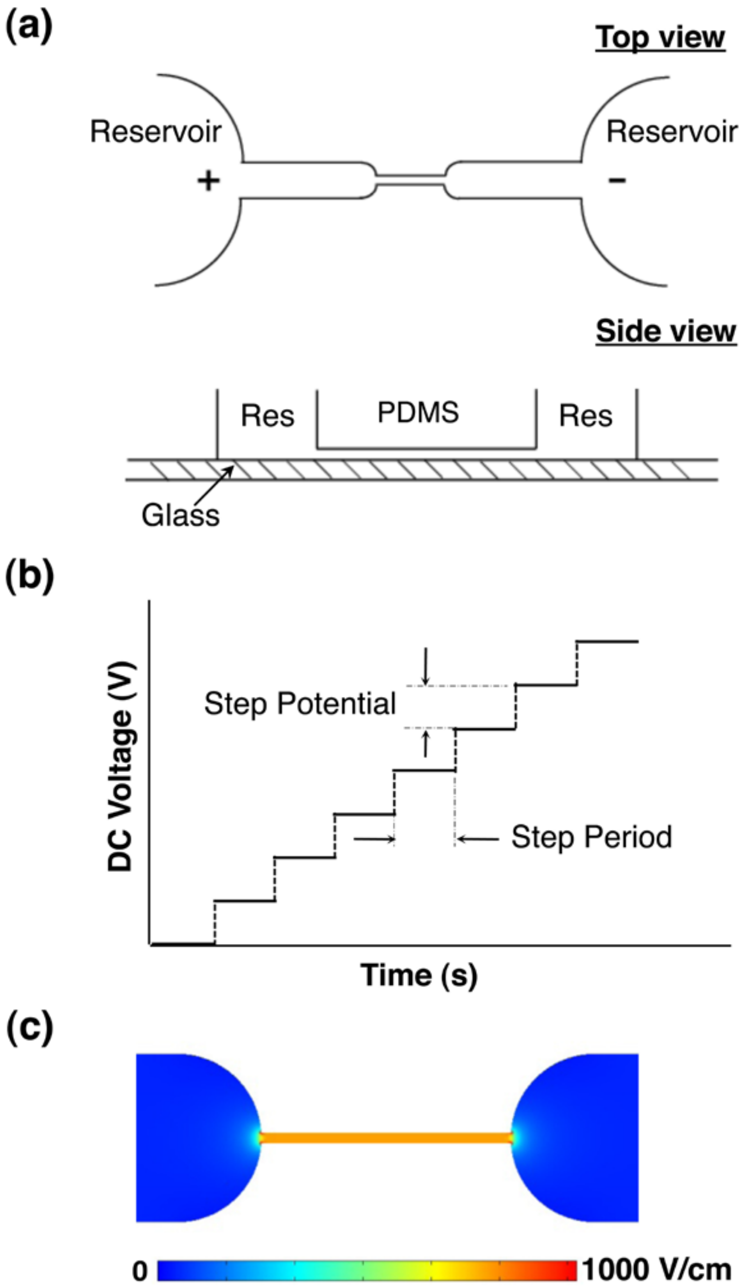

Figure 7. Microfluidic channels for separation of short ssDNA. (a) Schematic top and side views of the microfluidic device. The widths of the narrow and wide sections of the channel are 50 µm and 500 µm, respectively. The depth of the microchannel is around 35 µm. The total channel length is about 5 mm and the length of the middle narrow part is about 1 mm. The reservoirs (~ 3 mm in diameter) are made at both ends of the channel. (b) The DC potential in a staircase waveform applied to the microchannel. (c) Simulated electric field profiles in the microchannel (with a potential drop of 100 V). A uniform electric field is obtained in the middle region of the channel.

3.3 DESIGN OF THE MICROCHANNEL AND MODELING OF THE ELECTRIC FIELD DISTRIBUTION IN THE MICROCHANNEL

In this study, geometric variation was applied to a microfluidic channel to create a local high electric field in a geometrically defined section. The overall voltage across the channel was controlled to generate high electric field intensity in the defined section. The dimensions of the microfluidic channel (Figure 8) are: L_1=1 mm, L_2=2 mm, D_1=50 μm, D_2=500 μm. When a dc voltage V is applied to the buffer-filled channel, the potential drop at individual sections of the channel is proportional to its resistance within the section. The resistance of a certain section of the microchannel depends on the length, conductivity, and cross section area. For a channel with a uniform depth and varying width, the electric field strength is different in different section. The electric field strength in the narrow section E_1 and in the wide section E_2 can be roughly calculated according to the following equations:

$$\mathbf{E_1} = \frac{V}{2L_2(D_1/D_2)+L_1} \tag{4}$$

$$\mathbf{E_2} = \frac{\mathrm{V}}{\mathrm{L_1(D_2/D_1)+2L_2}} \tag{5}$$

The width D_1 is much smaller than the width D_2 in our study, which leads to much higher electric field strength in the narrow section than those in the wide sections when a dc voltage is applied across the overall length of the microchannel.

Modeling of the electric field distribution in the microchannels with different configurations was performed using Conductive Media DC model in COMSOL Multiphysics. We assumed no ion concentration gradient in the flowing fluid carrying the current and no presence of heating. The continuity equation $\nabla\cdot J=Q$, in which J is the current density, and Q is the current source. Here, J and Q are defined as $J=\sigma E$ and $E=\nabla V$ (E is the electric field and V is the applied dc voltage). With the absence of the current source, the Poisson's equation reduces to Laplace equation $\nabla\cdot(-\sigma\nabla V)=0$, where σ is the conductivity. The buffer used in our experiment is isotropic and the conductivity σ is lower than 100 PS/cm. The boundary conditions are as following:

1. $n\cdot J=0$ (electrically insulated) at $Y=\pm250$ μm in wide sections and $Y=\pm25$ μm in narrow sections.

2. V=the applied voltage at X=5 mm and V=0 at X=0 mm.

Here, the central axis and the left end of the microchannel are designated as Y=0 and X=0.

The modeling of the electric field strength in different configurations when a constant dc voltage across the channel is applied suggests that the field strength in the narrow section could reach about ten times higher than that in the wide section as the lengths of the narrow section and wide sections are regulated carefully.

The current was stable in the microchannels. The joule heating can be estimated based on the current and applied dc voltage. In the worse case, the joule heating can introduce around 4K increase in the temperature of the solution, assuming no dissipation of the heat. The actual temperature increase in the solution would be lower than this due to the dissipation of the heart through the channel walls and the cooling system fixed below the micro-device.

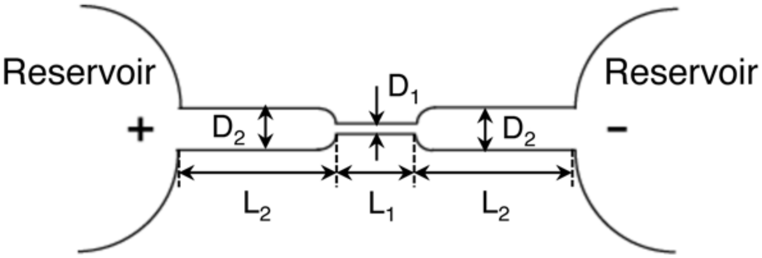

Figure 8. Configuration and dimensions of the microfluidic channel

3.4 MATERIALS AND METHODS

3.4.1 Fabrication of microfluidic channels

Microfluidic devices were fabricated by bonding a glass slide to a polydimethylsiloxane (PDMS) replica of a photoresist/silicon master mold with defined microchannels (Figure 3-3). The patterns of the microchannels were drawn by using a CAD software and printed with high resolution (10,000 dpi) on a transparency. The patterns were then transferred by photolithography to a photoresist film (SU-8 2000) spin-coated on a silicon wafer. After the photoresist was developed and baked, the photoresist/silicon wafer was used as a master mold for making PDMS replicas. PDMS prepolymer and curing agent (Sylgard 184, Dow Corning Corp.) mixed at a 10:1 (w/w) ratio were poured onto the photoresist/silicon master mold and placed in a vacuum desiccator for 1 h to eliminate all air bubbles. PDMS was then thermally cured in an oven for 3 h at 70 °C. After cooling, the PDMS replica was gently peeled off from the master mold and the dimension of the microchannels on the PDMS replica was measured by using a surface profilometer. Reservoirs (3 mm in diameter) were punched at both ends of the microchannels. The PDMS replica was then cleaned extensively with acetone and ethanol sequentially, and blown dry with nitrogen. The glass slide was cleaned in piranha solution (made by mixing H_2SO_4 and 30 w.t.% H_2O_2 in a volume ratio of 7:3, **CAUTION:** Piranha solution is a strong oxidant and must be handled with extreme caution) for 30 min at 80 °C and then rinsed with deionized water and blown dry. The PDMS replica was oxidized in oxygen plasma and then bonded with the pre-cleaned glass slide to form an enclosed microchannel with open reservoirs.

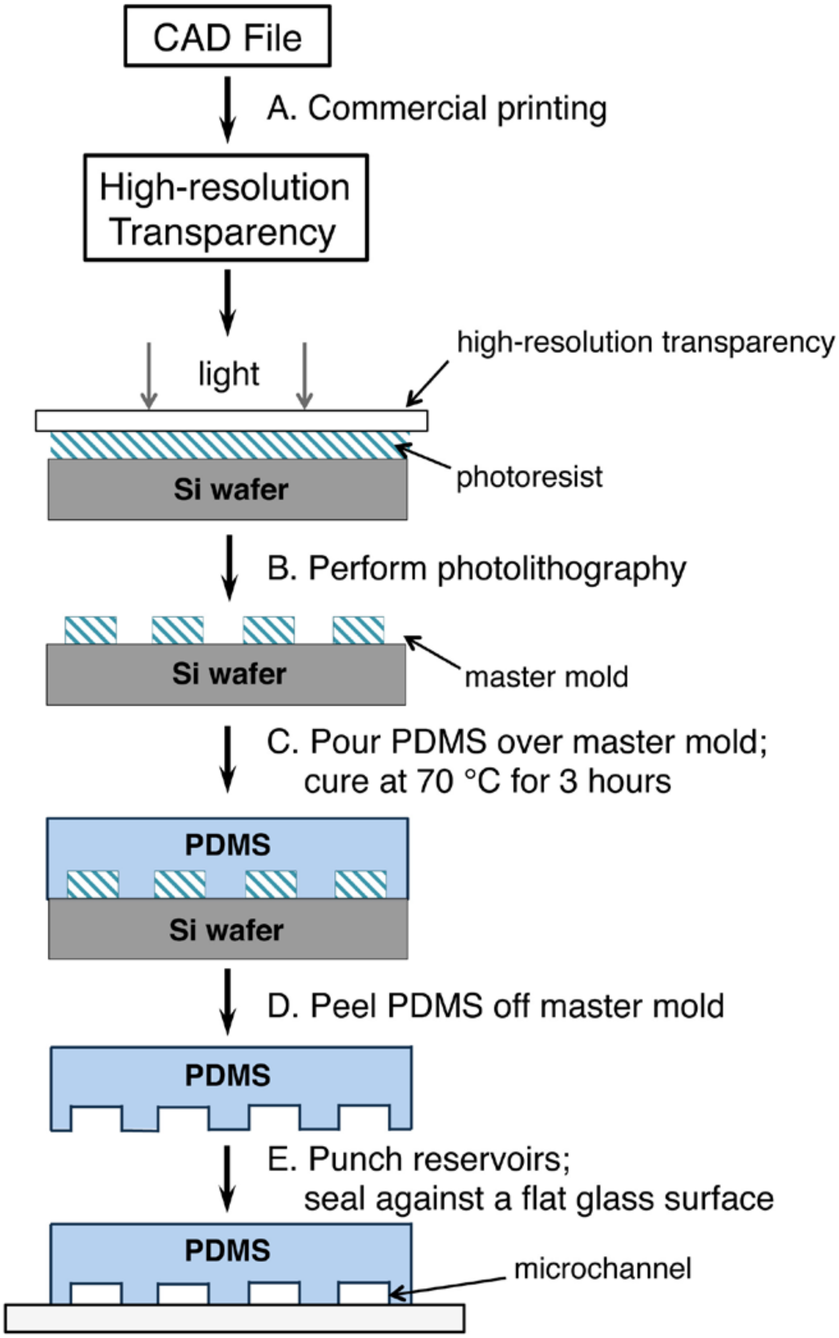

Figure 9. Scheme for fabricating microfluidic channels. A system of channels is designed using a CAD software. (A) The CAD file is printed with a commercial printer to produce a high-resolution transparency (10,000 dpi). (B) This transparency is used as a photomask in photolithography to produce a master mold, which consists of a positive relief of photoresist on a silicon wafer. (C) Liquid PDMS pre-polymer is poured over the master mold and cured for 3 h at 70 °C. (D) The PDMS replica is peeled from the master mold, and (E) reservoirs are punched at both ends of the channels and the PDMS replica is sealed to a flat glass surface to enclose the microchannels.

3.4.2 DNA samples

Fluorophore-labeled ssDNA fragments in 4 different lengths (60-nt, 70-nt, 80-nt and 90-nt) were used to demonstrate the efficiency of the new separation method. Sequences of these ssDNA fragments are listed in Table 1. They all have a common tail of 15 bases long at the 5' end, which is used to hybridize with a common probe. The DNA probe is modified with biotin at the 5′ end and has the following sequence: 5' biotin-TTT ATA AT*G ATG AAT TTA ATA TT*-3'. The 15 italicized bases in the sequence are complementary to the common tail of each ssDNA fragment.

DNA samples were obtained from Integrated DNA Technologies, purified using HPLC by the manufacturer, and used as received. Hybridization was performed at 25°C for 12 h by mixing equal molar quantities of ssDNA fragments and the biotinylated DNA probes in 5× SSC buffer (750 mM NaCl, 75 mM sodium citrate, pH 7.0) with a final DNA concentration of 2 µM.

Table 1. Base sequences of the DNA probe and the ssDNA fragments separated in our experiments

Name	Sequence
90-nt DNA *oligonucleotides*	5' Alexa 488-*AAT ATT AAA TTC ATC* TTC TGT CCC TTC CCA GAA AAC CTA CCA GGG CAG CTA CGG TTT CCG TCT GGG CTT CTT GCA TTC TGG GAC AGC CAA-3'
80-nt DNA *oligonucleotides*	5' Cy5-*AAT ATT AAA TTC ATC* TTC TGT CCC TTC CCA GAA AAC CTA CCA GGG CAG CTA CGG TTT CCG TCT GGG CTT CTT GCA TTC TG-3'
70-nt DNA *oligonucleotides*	5' Cy5-*AAT ATT AAA TTC ATC* TTC TGT CCC TTC CCA GAA AAC CTA CCA GGG CAG CTA CGG TTT CCG TCT GGG CTT C-3'
60-nt DNA *oligonucleotides*	5' Alexa 488-*AAT ATT AAA TTC ATC* TTC TGT CCC TTC CCA GAA AAC CTA CCA GGG CAG CTA CGG TTT CCG-3'

3.4.3 Immobilization of DNA samples in the microchannel

The cleaned and oxidized glass bottom surface of the microchannel was silanized with 2% (v/v) 3-aminopropyltriethoxysilane (APTES) in anhydrous ethanol. The reaction was carried out by continuously infusing APTES solution through the microchannel at a flow rate of 10 µL/min for 1 h at room temperature. The microchannel was then rinsed by flowing anhydrous ethanol, dried by blowing N_2 through, and baked at 90 °C for 2 h. Afterwards, the microchannel was treated with 2.5% (v/v) glutaraldehyde in PBS for 1 h at 37 °C, followed by rinsing with phosphate buffered saline (PBS). A solution of 0.2 mg/mL streptavidin was introduced into the microchannel and incubated at 4 °C overnight, and the reaction was quenched by flowing 50 mM ethanolamine in PBS through the channel. The microchannel was then filled with a blocking buffer (3 % BSA in PBS) for 45 min. To immobilize the DNA samples onto the bottom surface of the microchannel, ssDNA hybridized with the probe at a concentration of 2 µM were loaded into the microchannel and incubated for 3 h at 10 °C prior to the separation experiment. Schematic illustration of the immobilization of DNA samples in the microchannel is shown in Figure 10. The excessive DNA samples were washed out by a washing buffer (0.1 % Tween 20 in PBS) and a stretching buffer (20 mM histidine, pH 7.0, Sigma-Aldrich) sequentially.

3.4.4 Fluorescence image acquisition

The microfluidic device was mounted on the stage of a fluorescence microscope (Carl Zeiss Axioimager A1) for real-time fluorescence imaging. The fluorescence microscope was focused on the bottom surface in the middle zone of the microchannel. The shutter of the microscope was programmed and synchronized with the DC voltage source, so that images were taken after each step of the staircase function. In a typical experiment, DNA fragments in two sizes were labeled with two different fluorophores, which were imaged simultaneously through two fluorescent channels of the microscope.

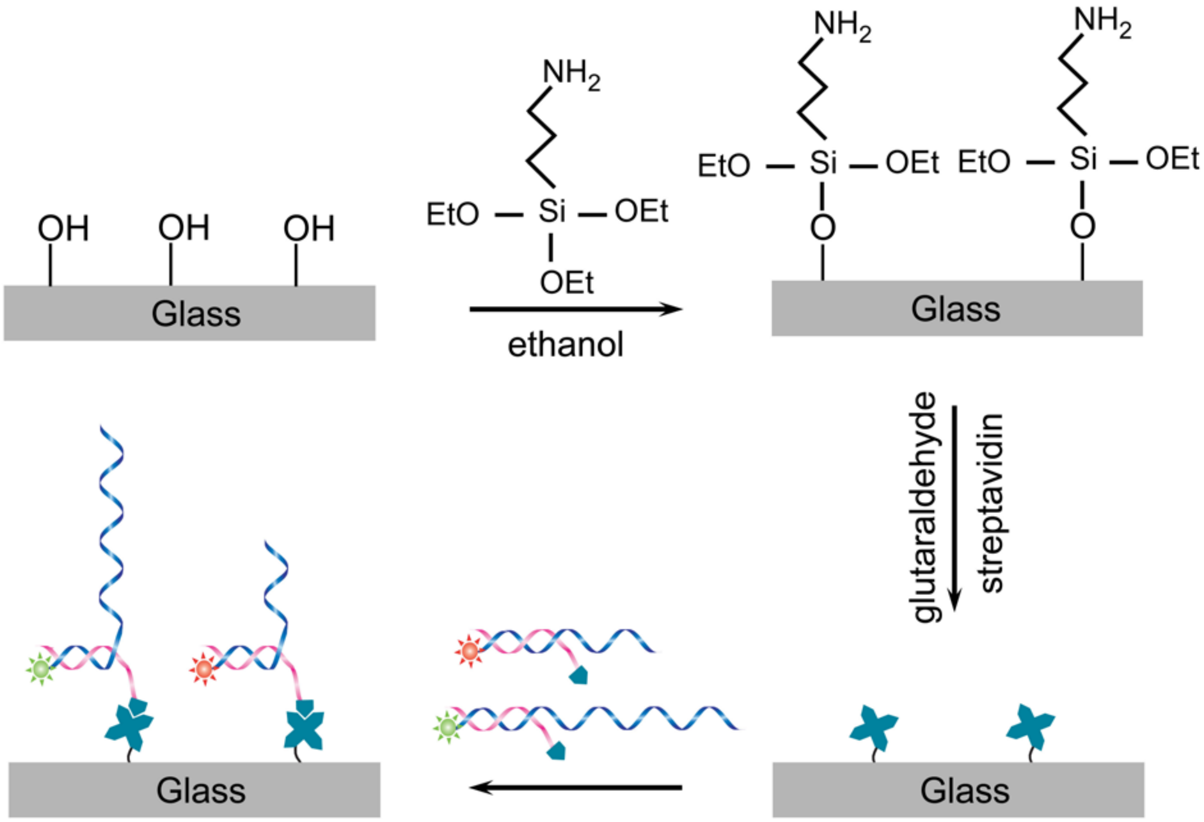

Figure 10. Schematic illustration of the immobilization of DNA samples in the microchannel.

3.5 RESULTS AND DISCUSSION

The microchannel allows us to stretch the short DNA fragments in a strong electric field with negligible Joule heating effect. Under our experimental conditions, the electric current in the buffer is less than a few microamperes even at the highest electric field strength (~6 kV/cm) applied in this study. A simple energy balance calculation suggests that the temperature rise of the buffer solution caused by Joule heating is less than 3 °C throughout the entire experiment (as the electric field increases stepwise from 0 to 6 kV/cm), assuming there is no heat dissipation to the surrounding environment. The actual variation of the solution temperature, as measured by a thermal couple, is less than 1 °C throughout our experiment, which suggests that the influence of Joule heating can be safely neglected in our analysis.

Figure 11a presents the normalized fluorescence intensities (α) obtained from ssDNA in 4 different lengths (90-nt, 80-nt, 70-nt and 60-nt) as a function of the electric field strength (E), where the fluorescence intensities have been normalized between 0 and 1 (by setting the initial intensity as “1”). In all experiments, α remains stable until E reaches a value that is sufficient to induce unzipping of the ssDNA tail from the short probe, upon which α undergoes a rapid decay to less than 5% of the initial intensity, indicating that most of the ssDNA fragments at a particular length have been removed. The decay of α is clearly length-dependent. Figure 3b presents the negative derivative of α ($-d\alpha/dE$), which corresponds to the amount of ssDNA detached from the surface, as a function of E. Four distinct peaks located at 2625, 3040, 3530, and 4315 V/cm are clearly visible, corresponding to ssDNA fragments of 90, 80, 70, and 60 nt, respectively.

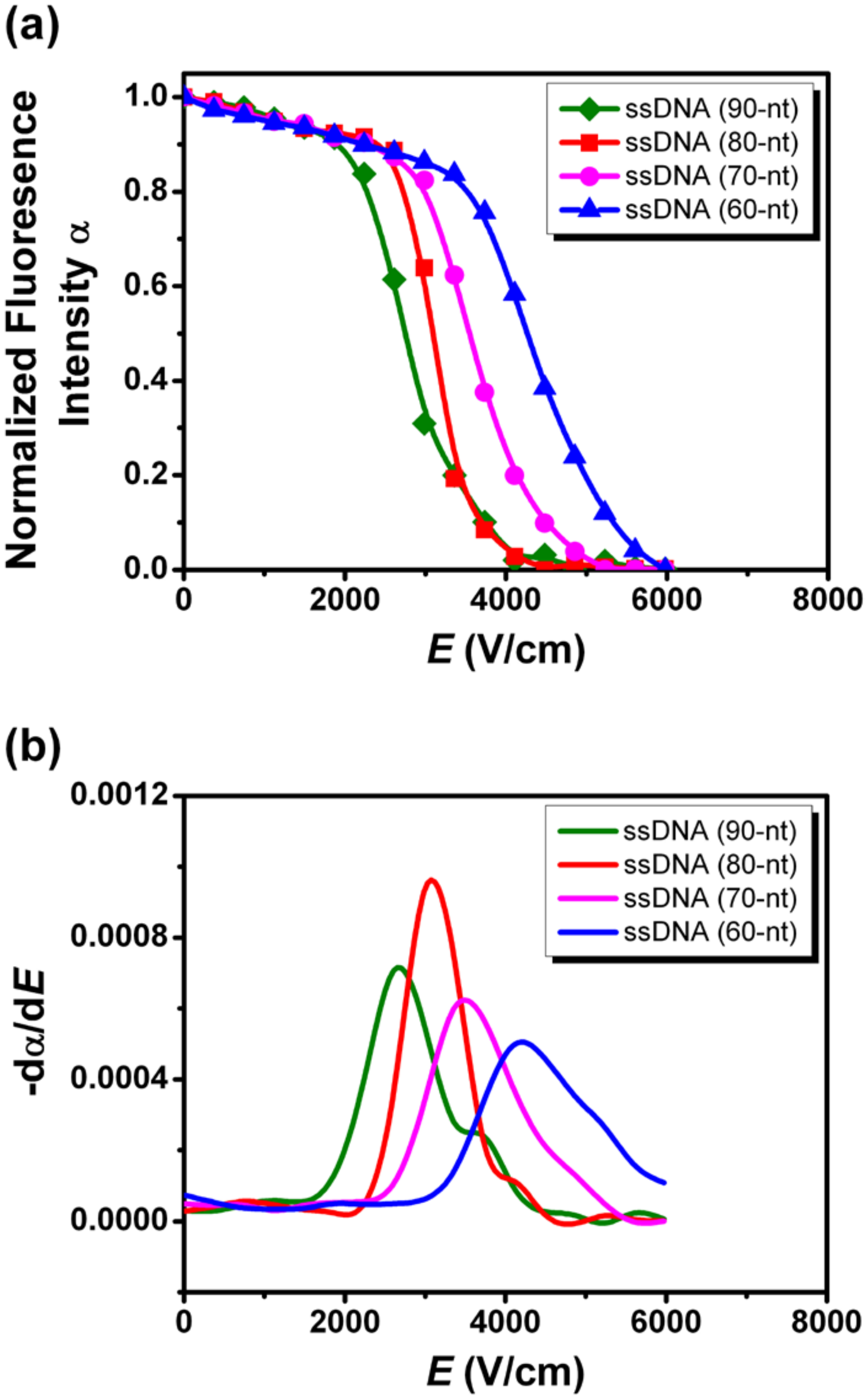

Figure 11. ssDNA separation results. (a) Normalized fluorescence intensities (α) obtained from the 90-nt, 80-nt, 70-nt and 60-nt ssDNA fragments as a function of the electric field strength (*E*). (b) Negative derivative of α (-dα/d*E*), which corresponds to the amount of ssDNA detached from the surface, as a function of *E*.

Based on the data presented in Figure 11, several perspectives may be concluded: i) experimental results show that detachment of ssDNA happens within a certain range of electric field instead of at a single critical point, which confirms that fluctuation force f becomes notable during the separation of short DNAs and thus interferes with the separation efficiency; ii) except at large electric field, the dependence of (-dα/dE) versus E presents Gaussian analogue distributions; and iii) the values of electrical field E that corresponds to the maximum of -dα/dE vary with the DNA chain length. These perspectives may be understood by an analysis of the fluctuation forces on tethered DNA chains.

The Gaussian analogue distributions of (-dα/dE) versus E as showed in Figure 11 is due to the fluctuation force stemming from the solvent effect.[111] The fluctuation force contributes to the total stretching force f_s, i.e., $f_s = f + qNE$. Here f is the component of fluctuation force along the direction of static electrical force, and q is the net charge on each nucleotide while N stands for DNA chain length. If we denote the threshold critical force that breaks the hybridization between tested DNA and DNA probe as f_t, then the DNA detachment should be conditioned as

$$f_t = f_s = f + qNE \tag{6}$$

Clearly, when the fluctuation force $f \geq f_t - NqE$, the DNA detachment occurs otherwise not. The normalized fluorescence intensity (α) measures the amount of DNA chains remaining at the surface under an electric field (E). This quantity is directly connected to the probability of the a single DNA chain detached from the surface, or equivalently, the probability of the stretching force exceeding the critical force of DNA departure. Given an electric field and a tethering condition, the critical fluctuation force to remove a DNA chain is given by

$$\boldsymbol{f_c = f_t - NqE} \tag{7}$$

If we let α=0 for the DNA departure from the surface and α=1otherwise, the probability of a DNA chain remaining at the surface can be obtained by integrating the probability density for $f < f_c$, i.e.,

$$\boldsymbol{\alpha(E) = \int_{-\infty}^{f_c} \rho\,(f) df} \tag{8}$$

where $\rho(f)$ is the probability density for the distribution of the fluctuation force. A derivative of Eq.(8) with respect to E gives

$$\boldsymbol{-\frac{d}{dE}\alpha(E) = Nq\rho(f_c) = Nq\rho(f_t - NqE)} \tag{9}$$

Eq. (9) is formally exact, independent of any specific experimental condition and DNA model that used in relative theoretical analysis. It states that, for any given DNA chain (thus N is fixed), the relation (-dα/dE) versus E is determined by probability density of fluctuation force $\rho(f_c)$.

In our previous work,[111] we have derived an analytical expression for $\rho(f)$ by using Gaussian chain models tethered on a hard wall. Figure 12 shows the theoretical predictions for the fluctuation force distribution versus the electric field for four representative DNA chain lengths. These curves suggest that the probability density of fluctuation force $Nq\rho(f_t - NqE)$ presents the analogue distribution, which can explain the shape of experimental data $-d\alpha / dE$ in Figure 11. For efficient separation of two DNA chains close to each other, the critical electric field, i.e., the expected value of $-d\alpha / dE$, should be different. According to Eq.(9), we have

$$\boldsymbol{E_m(N) = -\int E\frac{d\alpha(E)}{dE}dE = -\int [f_t - (f_t - NqE)]\rho(f_t - NqE)dE}$$

$$\boldsymbol{= \frac{1}{Nq}\int [f_t - f]\rho(f)df = \frac{f_t}{Nq} - \frac{f_m(N)}{Nq}} \tag{10}$$

In Eq. (10), $f_m(N)$ is the value corresponding maximum of $\rho(f)$. Although $f_m(N)$ is proven to vary with chain length N when N is relatively small, its value is generally much smaller than f_t, i.e., $E_m(N)$ is dominated by f_t / qN. This argument not only can explain the trend of $E_m(N)$ with chain N indicated in Figure 11, but also indicates that the resolution of DNA separation is closely related to the anchor design. The larger f_t, the higher resolution. Larger f_t may be realized, for example, by designing the probe in such a way that the 3' end of the probe will be immobilized onto the substrate (instead of the 5' end currently immobilized) in Figure 6. In this case, the hydrogen bonds between the bases of the ssDNA and the probe need to be broken almost simultaneously instead of in an avalanche manner (when the ssDNA unzips from the probe), and thus a much larger f_t is required in order for the ssDNA to depart from the surface. However large f_t requires a stronger electrical field to load the DNA, which, on one hand, brings the experimental difficulty as we explained above, and on the other hand, may cause DNA overstretching.

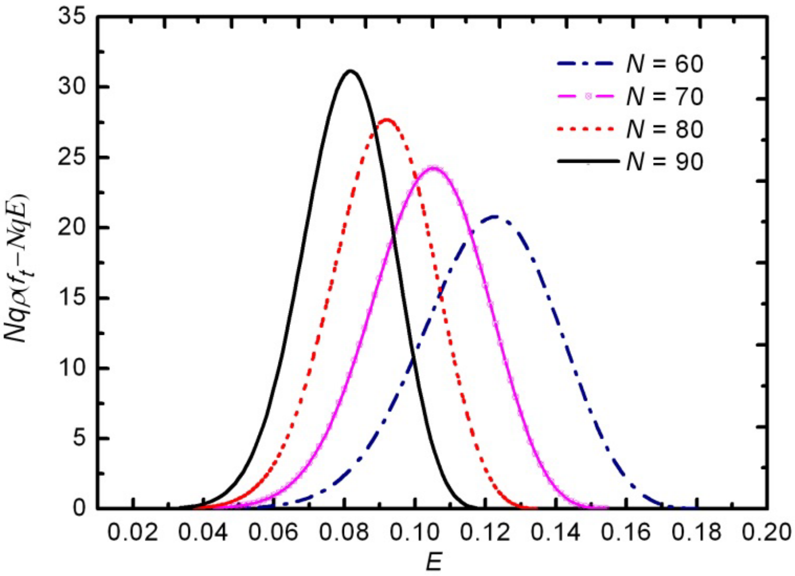

Figure 12. Analytical results for $Nq\rho(f_t - NqE)$ versus electric filed E with Gaussian chain model tethered on hard wall.[111] Here the unites for $Nq\rho(f_t - NqE)$ and for E are $(\beta aq)^{-1}$ and (βaq) with $\beta = 1/(k_B T)$ defined by the Boltzmann constant k_B and absolute temperature T, and a is the Kuhn length in Gaussian chain model which presents the effective size of each segment. N here stands for the number of segment.

3.6 CONCLUSIONS

In summary, we have demonstrated a proof-of-concept experiment for separation of short ssDNA by first tethering the ssDNA fragments onto a solid surface and then stretching them under an electric field in a microchannel. ssDNA fragments in four different lengths have been separated with a 10-nt resolution. Theoretical analysis indicates that the separation resolution is limited by the fluctuation forces on tethered DNA chains, which agrees well with experimental results. Compared with DNA separation by classic electrophoresis, this method has the following advantages: i) no polymer matrix is required, ii) key steps of separation may be accomplished in seconds and there is still much space for increasing the speed of operation by increasing the voltage ramping speed, iii) recovery of the separated DNA strands is straightforward—they can be directly taken out by the buffer flowing out of the microchannel, and iv) the microfluidic platform is convenient for automation and high-throughput applications.

4.0 SORTING SHORT FRAGMENTS OF SINGLE-STRANDED DNA WITH AN EVOLVING ELECTRIC DOUBLE LAYER

We have designed an integrated microfluidic platform with narrow microfluidic channels and low conductivity buffer, which were used to provide very high electric field strength and lessen the Joule heating. This system was proven to have the capability to separate between ssDNA fragments (< 100 nt) with a resolution of 10-nt. Here, we present a second approach for the discrimination of short DNA fragments by pulling the ssDNA off a noble charged metal surface, which uses the electric double layer to generate a strong electric field for pulling the ssDNA.

4.1 INTRODUCTION

Technological advances in micro/nanotechnology and high-resolution imaging systems empower the direct control of DNA molecules on surfaces by various means such as electric fields,[112, 113] hydrodynamic flows,[114] magnetic[115, 116] and optical tweezers,[117, 118] micropipettes,[119] and atomic force microscope (AFM) methods.[120, 121] Due to the intrinsic negative charges present on the DNA backbone, the use of an electric field is particularly powerful, efficient, and convenient to manipulate surface-immobilized DNA molecules in an aqueous solution. Electrical control of DNA molecules offers many advantages since they can be readily implemented in a massively parallel way, thus suitable for high-throughput and multiplexing tasks. In particular, electrode-tethered DNA molecules can be efficiently manipulated at very low applied electrode potentials, taking the advantage of the couterion-screened electric field that is significant within only few Debye lengths from the surface. Despite the extremely strong electric field at the electrode/solution interface, the electric current is limited to a capacitive, non-Faradaic charging process. Such approaches have been successfully utilized for dynamic electrical switching of DNA layers[122] with applications in the highly sensitive label-free sensing of specific DNA sequences and proteins,[123, 124] accelerating hybridization and selectively melting of mismatched DNA duplex,[125, 126] and measurement of electrically induced conformational changes of end-tethered DNA molecules on electrode surfaces.[127-129]

Previously we have reported a novel DNA separation method by tethering DNA chains to a solid surface and then stretching the DNA chains with an electric field.[105, 111, 113] The anchor is such designed that the critical force to detach the DNA strand is independent of the chain length. Because the stretching force applied to the DNA strand is proportional to the net charge, a gradual increase of the electric field leads to a size-based separation of the DNA strands. Efficient separation of lambda DNA (48,502 base pairs) from human genomic DNA (> 100,000 base pairs) has been demonstrated using this method.[105] However, when this method is applied to separation of short single-stranded DNA (ssDNA), e.g. with less than 100 nucleotides, a very strong electric field (on the order of 10^5 V/m) is needed to pull short DNA strands off the substrate. In practice, applying such a strong electric field may cause various technical problems such as Joule heating and side electrochemical reactions. Previously, we have used microfluidic narrow channels filled with a buffer of low ionic conductivity to apply such a strong electric field along the microfluidic channels (with negligible Joule heating) for separation of ssDNA tethered to an insulating glass surface of the channels.[113] Here we demonstrate a new procedure for separation of short ssDNA fragments by taking the advantage of the strong yet evolving non-uniform electric field near the Au surface in contact with a buffer solution which is gradually diluted by deionized water.

We show that by tethering the ssDNA to an Au electrode and applying a relatively low electrode potential on the Au electrode, ssDNA strands of different lengths can be separated by gradually diluting the buffer solution in contact with the Au electrode. The high electric field strength inside the electrical double layer at the gold/electrolyte interface allows us to pull short ssDNA strands off the surface with a very low electrode potential. Electrochemical reactions are avoided by maintaining the low electrode potential within the ideally polarizable region. Tuning the ion concentration of the electrolyte solution allows regulation of the non-uniform electric field. By gradually decreasing the ion concentration, longer ssDNA strands are detached first and then followed by the shorter ones. A numerical analysis based on a simple electric double layer model provides semi-quantitative explanations of the experimental results.

4.2 THEORETICAL DESCRIPTION OF THE ELECTRIC DOUBLE LAYER (EDL)

4.2.1 Potential distribution in EDL

In general, charging an electrode surface that is in contact with electrolyte solution induces a redistribution of the dissolved ions in solution, the so-called “electric double layer” (EDL), which eventually screens the electrode charge.

To calculate the potential distribution in the EDL at a charged surface, the electrochemical potential $\tilde{\tilde{\mu}}_i$ of ion i in a liquid phase at constant pressure and temperature has to be considered,[130, 131]

$$\tilde{\tilde{\mu}}_i = \tilde{\mu}_i + z_i F \psi = \tilde{\mu}_i^{\,0} + RT \ln(\gamma_a c_i / c^0) + z_i F \psi \tag{11}$$

where $\tilde{\mu}_i$ is the chemical potential, F is the Faraday constant, ψ is the electric potential due to the surface charge, $\tilde{\mu}_i^{\,0}$ is the standard chemical potential of ion *i* at constant pressure and temperature, R is the gas constant, T is the temperature, γ_a is the activity coefficient, c_i is the molar concentration of ion *i*, and c^0 is the standard molarity of 1 mol·l^{-1}. At equilibrium, the electrochemical potential of the ions must be the same everywhere (i.e. grad ($\tilde{\tilde{\mu}}_i$=0), and the electrical and diffusion force on the ion *i* must be balanced, [130, 131]

$$\nabla \tilde{\mu}_i = -z_i F \nabla \psi \tag{12}$$

where $\nabla = grad$. Insertion of the chemical potential $\tilde{\tilde{\mu}}_i = \tilde{\mu}_i^{\,0} + RT \ln(\gamma_a c_i / c^0)$ into Eq. (12), and its integration from a point in the bulk solution where $\psi = 0$ and $n_i = n_i^{\infty}$ and the bulk volume density $n_i^{\infty} = 1000 N_A c_i$, leads to the Boltzmann equation, giving the local concentration of each type of ion in the diffuse layer,[130, 131]

$$n_i = n_i^{\infty} \exp(-z_i e \psi / k_B T) \tag{13}$$

with k_B the Boltzmann constant and the conversion $e/k_B = F/R$ is applied. The volume charge density ρ of all ions present in the neighborhood of the surface is given by

$$\rho = e \sum_i n_i z_i \tag{14}$$

One further important equation is required, the fundamental Poisson equation, giving the net excess charge density at a specific distance from the surface:[130, 131]

$$\nabla^2\psi = \frac{d^2\psi}{dz^2} = -\frac{\rho}{\varepsilon_0\varepsilon_r} \tag{15}$$

where $\nabla^2\psi = div(grad\,\psi)$ and z is the surface normal direction. Substituting Eq. (13) and (14) into Eq. (15). We obtain the complete Poisson-Boltzmann equation, which describes how the electrostatic potential due to a distribution of charged atoms varies in space,

$$\nabla^2\psi = \frac{d^2\psi}{dz^2} = -\frac{e}{\varepsilon_0\varepsilon_r}\sum_i n_i^\infty z^i \exp\left[-z_i e\psi(z)/k_B T\right] \tag{16}$$

4.2.2 Debye-Huckel approximation

The Poisson-Boltzmann equation is a second-order elliptic partial differential equation, and can be solved analytically by assuming that the surface potential is small everywhere in the EDL and by expanding the exponential (using the relation $e^{-\alpha} = 1-\alpha$ for small α), which leads to the Debye-Huckel approximation:[130-132]

$$\nabla^2\psi = \frac{d^2\psi}{dz^2} = k^2\psi(z) \tag{17}$$

where

$$k = \left(\frac{e^2\sum_i n_i^\infty z_i^2}{\varepsilon_0\varepsilon_r k_B T}\right)^{1/2} \tag{18}$$

k is called the Debye-Huckel parameter and is mainly dependent on the bulk volume density n_i^∞. The potential decays exponentially in the diffuse layer with the characteristic distance given by the Debye length $\lambda_D = k^{-1}$. This value corresponds to the thickness of the EDL, which increases with dilution.

4.2.3 Gouy-Chapman model

As the Debye-Huckel approximation is not valid for high surface potentials, the Poisson-Boltzmann equation has to be solved explicitly. Analytically, this can be done only under the assumption of a symmetrical electrolyte where the valence of the co-ion is equal to the valence of the counterion, leading to the Gouy-Chapman equation[127, 130-132]

$$\tanh[z_i\tilde{\psi}(z)/4] = \tanh(\frac{z_i\tilde{\psi}_S}{4})\exp(-kz) \tag{19}$$

where $\tilde{\psi} = e\psi / k_B T$ is the dimensionless potential.

At a flat charged metal surface, the resulting screened potential distribution as a function of distance from the surface on the solution side can be described by the Gouy–Chapman equation:

$$\Phi = \frac{2k_BT}{e} ln\left(\frac{1+\gamma\exp(-kx)}{1-\gamma\exp(-kx)}\right), \quad \gamma = tanh\left(\frac{e\Phi_0}{4k_BT}\right), \ k = \sqrt{\frac{2e^2\rho_0}{\varepsilon_r\varepsilon_0k_BT}} \tag{20}$$

where x is the distance to the surface, Φ_0 is the applied surface potential, e is the electron charge, ρ_0 is the average ion concentration, ε_r is the relative permittivity, ε_0 is the permittivity of free space, k_B is the Boltzmann constant, and T is the temperature.

The electric field is given by:

$$E = -\frac{\partial\phi}{\partial x} = -\sqrt{\frac{8\rho_0k_BT}{\varepsilon_r\varepsilon_0}}\sinh(\frac{e\phi}{2k_BT}) \tag{21}$$

4.2.4 Principle of DNA manipulation at charged metal surface

In this study, as described by the Gouy-Chapman model, the bulk of the potential in the double layer at the electrode surface is dropped over the Debye length λ_D, which is inversely proportional to the square root of the monovalent salt concentration. Due to counterion screening, strong localized electric fields can be generated within the double layer near the electrode surface by the application of a low voltage potential difference between two electrodes, where there is no Faradaic current and the electrodes can be treated as ideally polarizable. The enormous electric field within the Gouy-Chapman layer in the electrode surface region provides a powerful route for manipulation of DNA strands on the surface at low electrode potentials. By this it is possible to tune the magnitude of electrostatic stretching force acting on the DNA strands dependent on Debye length of the solution.

4.3 MATERIALS AND METHODS

4.3.1 Fabrication of gold electrode

P-type silicon (100) wafers (0.001 Ω·cm, from Siltronix Corp.) were first coated with a 10 nm Ti adhesive layer, and then a 200 nm thick of gold film by using electron beam evaporation (VE-180, Thermionics Laboratory Inc., U.S.A.). 10 mm × 10 mm pieces were cut from the gold coated wafer and used as electrodes. The electrodes were cleaned in Piranha solution (mixture of H_2SO_4 and 30 w.t.% H_2O_2 at a weight ratio of 7:3, CAUTION: Piranha solution is a strong oxidant and must be handle with extreme caution) for 10 min, thoroughly rinsed with deionized water (Millipore, 18.2 MΩ), and dried with nitrogen.

4.3.2 Oligonucleotide sequences

All oligonucleotides were purchased from Integrated DNA Technologies. The sequences of the DNA and probe are shown in Table 2. Both 60-mer and 90-mer oligonucleotides have no significant self-complementarity. The thiolated probe oligonucleotides were treated by adding 1 µM tris(2-chloroethyl) phosphate to disrupt formation of disulfide bonds between the thiol linkers.

Table 2. Base sequences of the thiolated DNA probe and ssDNA fragments

Name	**Sequence**
Thiolated DNA probe	5′ HS-$(CH_2)_6$-TT*GAAGATGAATTTAATATT*-3′
90-mer DNA *oligonucleotides*	5' Alexa 488-*AAT ATT AAA TTC ATC TTC* TGT CCC TTC CCA GAA AAC CTA CCA GGG CAG CTA CGG TTT CCG TCT GGG CTT CTT GCA TTC TGG GAC AGC CAA-3'
60-mer DNA *oligonucleotides*	5' Alexa 647-*AAT ATT AAA TTC ATC TTC* TGT CCC TTC CCA GAA AAC CTA CCA GGG CAG CTA CGG TTT CCG-3'

4.3.3 Immobilization of DNA probes on the gold electrode

Thiolated ssDNA probes (2 µM) were immobilized on the freshly prepared gold electrode in a high-salt buffer (1 M potassium phosphate buffer pH 7.0) through thiol-gold covalent bonding.

Immobilization was completed after 24 h incubation time at room temperature. Afterwards, the electrode was rinsed with deionized water. Mercaptohexanol (MCH) was then deposited onto the gold surface by exposing the electrode to an aqueous solution containing 1 mM MCH for ~20 min. The formation of a MCH layer passivates the gold electrode and reduces nonspecific interactions between DNA and the gold surface during the subsequent hybridization step.[133] The surface density of the ssDNA probes immobilized on the gold surface was quantified by a previously published electrochemical method.[134]

4.3.4 DNA hybridization

Before hybridization, the gold electrodes with immobilized ssDNA were thoroughly washed with deionized water. 1 μM target ssDNA in hybridization buffer (1 M NaCl, 10 mM phosphate buffer, pH 7.5) was applied onto the electrode and the electrode was incubated at 25 °C for 24 h. Finally, hybridized chips were rinsed with 0.1% Tween-20 in 1 M NaCl, 10 mM phosphate buffer (pH 7.5), and the hybridization buffer (1 M NaCl, 10 mM phosphate buffer, pH 7.5), sequentially.

4.3.5 Electric-field-induced DNA stretching and in situ fluorescence monitoring

Figure 13 schematically shows the custom-built electrochemical flow cell specifically designed for stretching DNA immobilized on the gold electrode and *in situ* fluorescence imaging of the gold electrode surface under an electric field. The gold electrode with immobilized DNA was used as the working electrode and an ITO-coated glass was the counter electrode. The distance between the working electrode and the counter electrode was 2.5 mm. The electrochemical cell was first filled with detection buffer of a high ionic strength (100 mM NaCl aqueous solution) and incubated for 10 min in the dark. Afterwards, a potential difference was applied between the two electrodes using a Keithley 6487 Voltage Source. The deionized water was continuously introduced into the flow cell at a rate of 60 μL/min and the temperature was kept at 15 ˚C. Departing of ssDNA from the surface was monitored in real-time by a fluorescence microscope (Carl Zeiss AxioImager A1). Fluorescence images were taken and analyzed using an image-analyzing software.

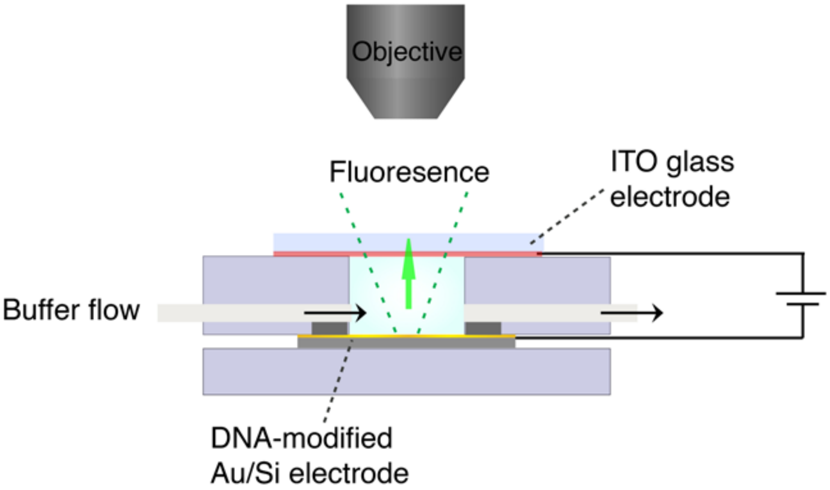

Figure 13. Schematic of custom-built electrochemical flow cell designed for stretching DNA immobilized on the gold electrode and *in situ* fluorescence imaging of the gold electrode surface under an electric field.

4.4 RESULTS AND DISCUSSION

Figure 14 schematically shows a typical procedure employed in our experiments for discrimination of DNA by stretching in an electric field near a charged gold surface. ssDNA probes were first immobilized to the gold electrode surface at a surface density of ~3×10^{12} /cm2 (Figure 14a). Then, fluorophore-labeled target ssDNA strands of different lengths, with a common tail of 18 bases long at the 5' end complementary to the ssDNA probe, were allowed to hybridize with the ssDNA probe on the gold surface (Figure 14b). Afterwards, the gold electrode was mounted in a custom-built electrochemical flow cell (shown in Figure 13) and a DC voltage (300 mV) was applied between the counter electrode and the gold electrode. The fluorescence intensity of the gold electrode surface was monitored in real time while reducing the ionic strength of the detection buffer solution by introducing deionized water into the channel at a flow rate of 60 μl/min. At this flow rate, the hydrodynamic force, compared to the electrostatic force, applied on the DNA strands can be neglected. With a potential drop at 300 mV across the cell, the current was limited to non-Faradic current, and thus the detrimental electrochemical reaction was avoided.

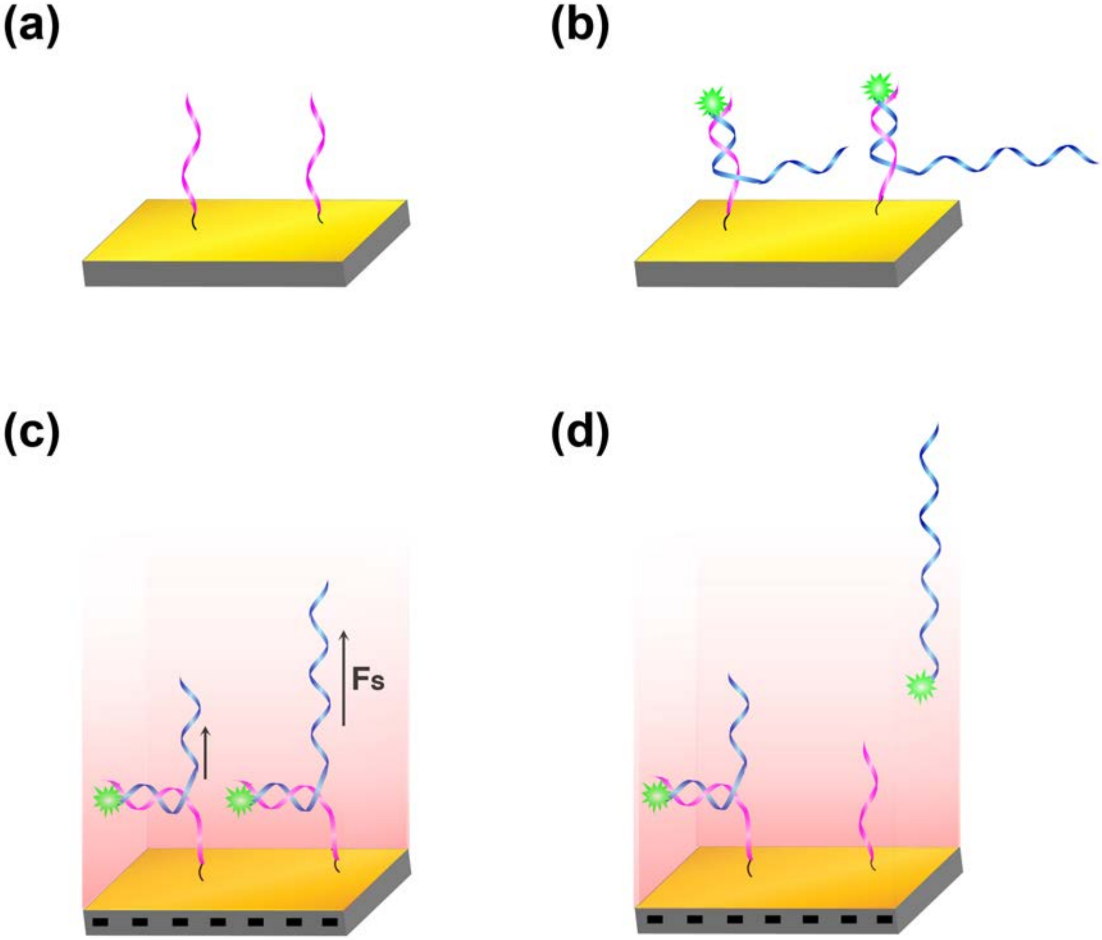

Figure 14. Schematic procedure for discrimination of DNA by stretching in an electric field near a charged gold surface. (a) ssDNA probes are immobilized to the gold electrode surface. (b) fluorophore-labeled target ssDNA strands of different lengths, with a common tail complementary to the ssDNA probe, hybridize with the ssDNA probe on the gold surface. (c) Electrically induced ssDNA unzipping from the probe immobilized on the charged gold electrode. (d) ssDNA strands are discriminated by length.

Figure 15a shows the fluorescence responses of 60-mer ssDNA and 90-mer ssDNA to a gradual reduction in the ionic strength of detection buffer with 300 mV potential drop across the cell. At high ionic strength (i.e. when the NaCl concentration in the buffer drops from 100 mM down to several mM), the fluorescence intensities of ssDNA strands of both lengths gradually decrease as the ionic strength decreases, but no significant discrimination is observed between the two plots. At about the 210th second, when the NaCl concentration to dropped to around 1.05 mM, the fluorescence intensity of the longer ssDNA (90-mer) starts to decay faster than that of the shorter one (60-mer) and the fluorescence response profiles of the two ssDNA strands are obviously separated.

Figure 15b shows the result of a control experiment, where the fluorescence responses of the ssDNA strands to a gradual reduction in the ionic strength of detection buffer are monitored without applying a potential drop across the cell. In this condition, it is found that the fluorescence response is independent of the ssDNA strand length. The normalized fluorescence intensity profiles of the two ssDNA strands are almost identical. The fluorescence signal remains constant as the ionic strength gradually decreases until around the 254th second when the ionic strength was reduced to 0.60 mM, after which the fluorescence intensity drops significantly for both ssDNA strands. The sudden drop of fluorescence intensity indicates that ssDNA strands of both lengths begin to dissociate from the probe and depart from the surface. This is likely because when the ionic strength decreases, the charges along DNA backbone become less shielded by counterions, therefore making the dsDNA duplex less stable.[135, 136]

Compared with the control experiment, stretching DNA near a charged Au surface can clearly discriminate ssDNA strands by length, when they are tethered to the surface by hybridizing one segment of the ssDNA to a probe immobilized on the surface. The different fluorescence responses observed when stretching the ssDNA strands of two different lengths may be explained by the following.

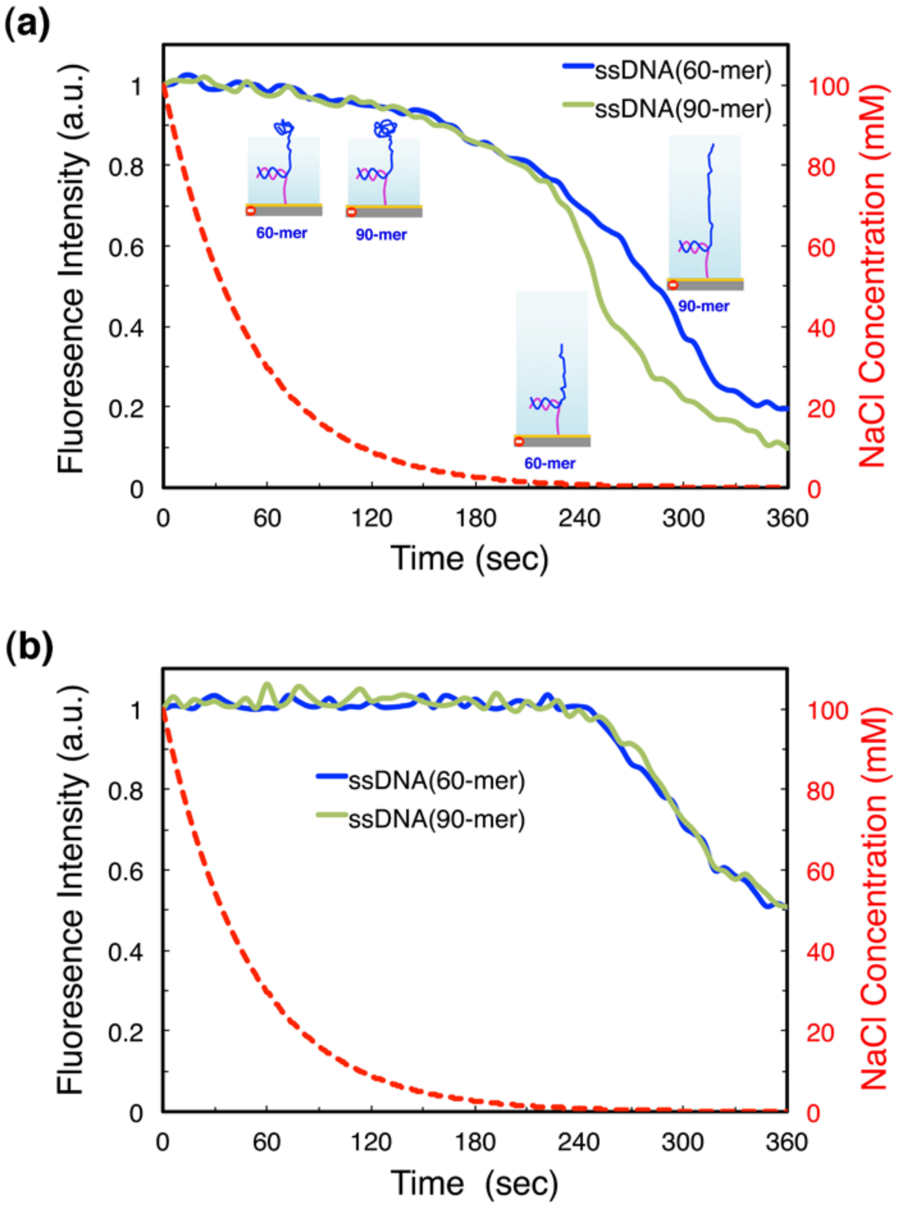

Figure 15. Fluorescence responses of 60-mer and 90-mer ssDNAs tethered to the gold surface as a function of buffer concentration. (a) 300 mV potential drop is applied acrossed the cell. (b) a control experiment (no potential drop is applied).

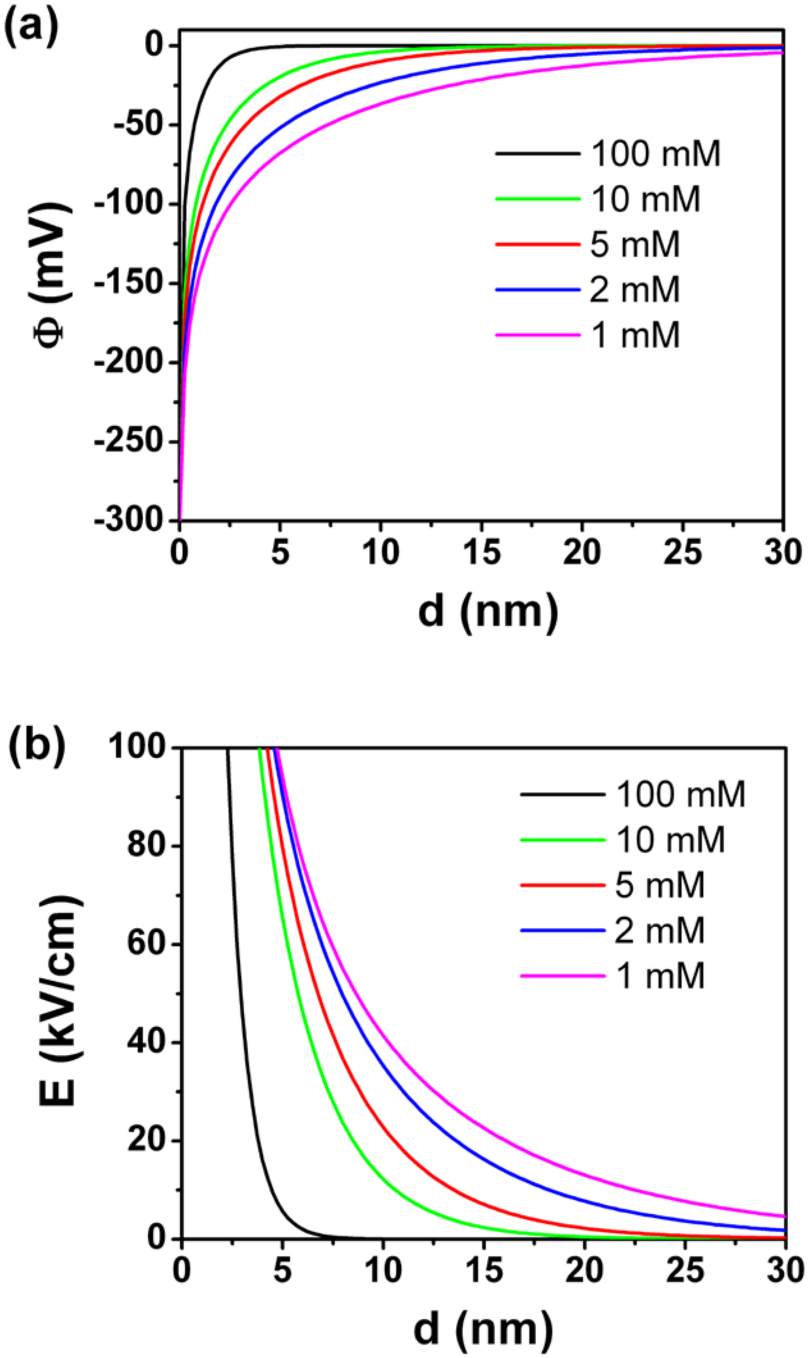

Figure 16. Gouy-Chapman potential **Φ** (a) and electric field (b) in the buffer solution plotted as a function of the distance ***d*** to the electrode surface that is biased at 300 mV. Curves are calculated for solutions containing varying concentrations of monovalent salt (NaCl).

Generally, an applied electrode potential results in the formation of an electrical double layer at the electrode surface, which screens the electric field so that it is confined at the electrode/solution interface. Figure 16 shows the Gouy-Chapman solutions of electric potentials and electric fields in the electrical double layer for varying concentrations of NaCl solution under the applied electrode potential Φ_0= 300 mV. The electrical double layer generates a large electric field within a few Debye lengths from the surface. Because of the rapid decay of the electric field, the electrical force exerted on the ssDNA strands becomes negligible beyond a few Debye lengths from the gold surface.

The fluorescence response of the ssDNA strands depends on the buffer ionic strength (as shown in Figure 15), which modulates the Debye screening length of solution. Reducing the ionic concentration increases the Debye screening length. In our system, target ssDNA strands are hybridized to the DNA probes, which are tethered onto the electrode surface via thiol anchors with low grafting density. The electrical stretching force interaction range scales with the Debye screening length. Thus, careful control of the solution ionic strength enables manipulation of the ssDNA conformations and the forces exerted on the hybridized ssDNA strands.

In solutions of high ionic strength, the Debye screening length is very small so that screening effects are extremely strong and the electrostatic potentials decay within only several nanometers. As a result, the electrostatic potential emanating from the surface is too short-ranged to affect the ssDNA strands considerably. Therefore, although the surface-proximal part of the DNA strands adopt a highly extended upright state, the major part of the ssDNA strands extend away from the electrode surface and lie outside of the electrical double layer. The ssDNA strands can be regarded as almost perfectly flexible chains with persistence length of the order of about 1 nm and thus adopt a random coiled conformation. In such a condition, the electric stretching forces loaded on either of the 60-mer and 90-mer ssDNA strands are not sufficiently large to unzip them from the surface so that their fluorescence intensities maintain constant.

In solutions of medium ionic strength, electric fields emanating from the charged surface have a significant influence on the surface-proximal part of the DNA strands. The electrode surface proximal part of the ssDNA strands resides in the strong electric field region, and thus is stretched by the electric forces, while the upper part of the ssDNA is not exposed to the strong electric field and its conformation is in a randomly coiled state. Because both ssDNA strands have the same length in the strong electric field region, the electric stretching forces exerted on both ssDNA strands are nearly identical. Reducing the ionic strength increases the Debye length, which leads to longer ssDNA segments lie in the strong electric field. When the stretching forces are sufficiently large, both ssDNA strands unzip from the DNA probes and are sequentially detached from the surface at the same time. The decay of fluorescence intensities of both ssDNA strands revealed the same behavior.

At lower ionic strength, the Debye screening length becomes much larger. Due to the weak screening effect, the electric field that emanates from the negative electrode surface extends over a very long range. The ssDNA strands become rigid and extremely extended so that they adopt almost upright conformation on the electrode surface with a certain tilt angle. In fact, the stiffening of ssDNA strands in solutions of low ionic strength has also been observed and explained by Kaiser et al.[127] and Murphy et al.,[128] and As a result, all segments of both ssDNA strands are inside the range of Debye screening electric fields, which results in both ssDNA strands being stretched by the electric forces. The 90-mer ssDNA strands possess more negative charges and thus are loaded with greater electric stretching forces than the 60-mer ssDNA strands. Consequently, the 90-mer ssDNA strands detach from the surface faster than the

60-mer ssDNA strands, which is indicated by the faster fluorescence intensity decay of 90-mer ssDNA.

4.5 NUMERICAL ANALYSIS

The different fluorescence responses observed when stretching the ssDNA strands of two different lengths may be explained by an electric double layer model in electrochemistry. In the presence of an electric potential, the Au electrode is in contact with an electric double layer (EDL) with a sharp decline of the electric field. The inhomogeneous electric field exerts a pulling force on the DNA chains due to the presence of the backbone charge.[137, 138] Apparently the magnitude of pulling force is not only related to the number of nucleotides (N) but also to the non-local electric field. Since the electric field varies with the ion concentration, which is time-dependent due to the introduction of deionized water, the pulling force, here designated as $F[N,t]$, depends on both time and the DNA chain length. Clearly, an explicit expression for $F[N,t]$ will provide insights into the separation mechanism and thus an explanation of the experimental results.

To seek a simple expression for $F[N,t]$, we assume that the tethered DNA chains are uncorrelated. Although a more accurate description can be obtained by, e.g., using the density functional theory,[139, 140] this assumption greatly simplify the problem at hand while it can still, as we shall see, provide meaningful insight into the experiment results. Under this assumption, the distribution of electric potential can be obtained by following the conventional knowledge of the electric double layer. Whereas it has been shown that the density functional theory provides a robust tool to investigate the electric double layer at various ion concentrations,[141, 142] we conjecture that the Poisson-Boltzmann (PB) equation provides an adequate description because the ion concentration is very small (less than 100 mM).[142]

In a coordinate system with the Au surface as the *xy* plane and the normal direction pointing to the solution as the z axis (see the inset of Figure 17), the electric potential changes only along the z direction. For NaCl solution near a planar electrode, the PB equation is given by

$$\frac{d^2\phi(z)}{dz^2} = \frac{2e\rho^0}{\varepsilon}\sinh\left[\frac{e\phi(z)}{k_B T}\right] \tag{22}$$

where ρ^0 is the salt concentration in the bulk, k_B is Boltzmann constant, T is the temperature solution, and $\varepsilon = \varepsilon_r \varepsilon_0$ is the dielectric constant. In this work, we take ε_r =82.0 for saline water.[143] Since the distance between two electrodes (Au surface and counter electrode) is on macroscopic level, it is reasonable to use the following boundary conditions:

$$\left.\frac{d\phi(z)}{dz}\right|_{z\to\infty} = 0; \qquad \phi(z)\big|_{z\to\infty} = 0; \qquad \phi(z)\big|_{z\to 0} = \phi^w \tag{23}$$

where ϕ^w denotes the surface potential. We can derive an analytical expression for the electric potential[144]

$$\phi(z) = \frac{2k_B T}{e}\ln\frac{1+\gamma e^{-\kappa z}}{1-\gamma e^{-\kappa z}}\,. \tag{24}$$

where $\kappa = (\frac{2\rho^0 e^2}{\varepsilon k_B T})^{1/2}$ is the Debye screening parameter, and $\gamma = \tanh[e\phi^w / (4k_B T)]$.

In our experiment, the ion concentration ρ^0 in the bulk varies with time. If we denote the volume of the solution confined within the electric double layer as V, and the average volume flow rate as v, the mass conservation equation within the cell is given by:

$$\rho^0(t+\delta t)V = \rho^0(t)V - \rho^0(t)v\delta t\,. \tag{25}$$

In writing the above equation, we assume that ion transport due to diffusion is negligible. In a differential form, Eq.(25) becomes

$$\frac{d\rho^0(t)}{dt} = -\frac{v}{V}\rho^0(t)\,. \tag{26}$$

An integration of Eq.(26) gives

$$\rho^0(t) = 100\exp(-0.0209t) \tag{27}$$

In deriving the above result, we have applied the boundary condition $\rho^0(0) = 100$ mM, $\rho^0(210) = 1.05$ mM, and $\rho^0(254) = 0.6$ mM. The ion concentration versus time is plotted in Figure 15. A combination of Eq.(24) and Eq.(27) gives the time-dependent electric potential distribution $\phi(z,t)$, which is presented in Figure 17 at three representative times ($t = 0$, 250, 300 s). While the contact value of electric potential is fixed by the applied surface potential, its gradient near the electrode surface varies sharply with the ion concentration.

To find the stretching force due to the varying electric field, we assume that each ssDNA chain is fully extended to the solution before detaching from the Au surface. In other words, we treat each ssDNA chain as a linear "cord" perpendicular to surface with a charge density $\sigma = q_e / \lambda$. Here q_e is the effective charge on each nucleotide, and λ is the average extension between two nucleotides (or inter-base distance in ssDNA). The total force pulling each chain can be calculated from

$$\begin{aligned} F[N,t] &= \sum_{i=1}^{N} q_e E[z_i,t] = -\sum_{i=1}^{N} q_e \frac{d\phi}{dz} = -\sum \sigma dz \frac{d\phi}{dz} \\ &= -\int_{z=L_0}^{z=L_0+N\lambda} \sigma d\phi(z,t) \\ &= \sigma[\phi(L_0,t) - \phi(L_0+N\lambda,t)] \end{aligned} \tag{28}$$

In Eq.(28), L_0 is the distance of the hybridized head of a stretched ssDNA chain to the surface, and its value is associated with the probe DNA. In this work, L_0 is assumed to be 1.5 nm. From the first line to second line in Eq.(28), we changed the discrete summation into a continuous function. Because ssDNA is very flexible, the contour length changes greatly at different conditions but the inter-base distance λ is relatively constant.[145, 146] Here we adopt λ=0.42nm[146] since the ssDNA sequence is partially hybridized with the probe DNA. The effective charge of each nucleotide may vary slightly in different conditions[138] and for saline water we take $q_e = -0.25e$.[137]

In Figure 18, we plot the time-dependent pulling force on 90-mer ssDNA and 60-mer ssDNA. As time elapses, the pulling force on both 90-mer ssDNA (the red curve) and 60-mer ssDNA (the black curve) increases, and they remain identical until around 180 seconds. After that, the pulling force on 90-mer ssDNA rises more quickly than that on 60-mer ssDNA before both reach their own plateaus. The difference in pulling forces explains why 90-mer ssDNA escapes from surface prior to 60-mer ssDNA.

The results shown in Figure 17 and Figure 18, as well as the pulling force expression in Eq.(28), explain the separation mechanism. Because the charge density on ssDNA is fixed, Eq.(28) indicates that the magnitude of the pulling force depends only on the electric potential across the span of a single ssDNA chain. To facilitate the discussion, we mark the end near surface as A, and the other one as B. The corresponding electric potentials are $\phi(z_A)$ and $\phi(z_B)$, abbreviated as ϕ_A and ϕ_B, respectively. Obviously, for different ssDNA chain, ϕ_A is independent of the chain length due to the identical probe design. At the beginning of experiment, the ion concentration is relatively high, and the effective length of the electric double layer to solution is much smaller than the extended lengths of both 90-mer and 60-mer ssDNA. In that case, ϕ_B is approximately equal to zero for both ssDNAs, and ϕ_A is finite but identical. Thus the pulling forces that proportional to $(\phi_B - \phi_A)$ are the same. As the ion concentration decreases, the thickness of electric double layer increases. If it is still less than the extended lengths of both ssDNAs, we hold $\phi_B = 0$, and $(\phi_B - \phi_A)$ still the same for different chains. As shown in Figure 17, the gradient of the electric potential become less sharp, and ϕ_A becomes more negative. That means in this period the strength of pulling force increases but still identical for both ssDNAs. When the effective length of electric field continues to increase, the head B of short ssDNA is covered by the electric potential, and ϕ_B has finite negative value for short ssDNA while still zero for long ssDNA. In this period, the potential drops for different lengths $(\phi_B - \phi_A)$ gradually become different, and the longer ssDNA undergoes a larger pulling force. If this pulling force is beyond the tethering force, the long ssDNA detaches from the electrode surface. Finally, if the ion concentration becomes sufficiently dilute, and the head B of long ssDNA is also covered by the electric potential, in that case, ϕ_B has finite and negative value for both short and long ssDNAs, but the value for short ssDNA is more negative, thus $(\phi_B - \phi_A)$ is smaller. In other words, the pulling force for long ssDNA is still larger than that for short ssDNA. In the limit case of infinite dilute ion concentration, the electric field $E = \phi^w / d$ with d the distance of two parallel layers, and pulling force for ssDNA simply becomes $q_e \phi^w N / d$, and the system recovers to our previous experimental design.[113]

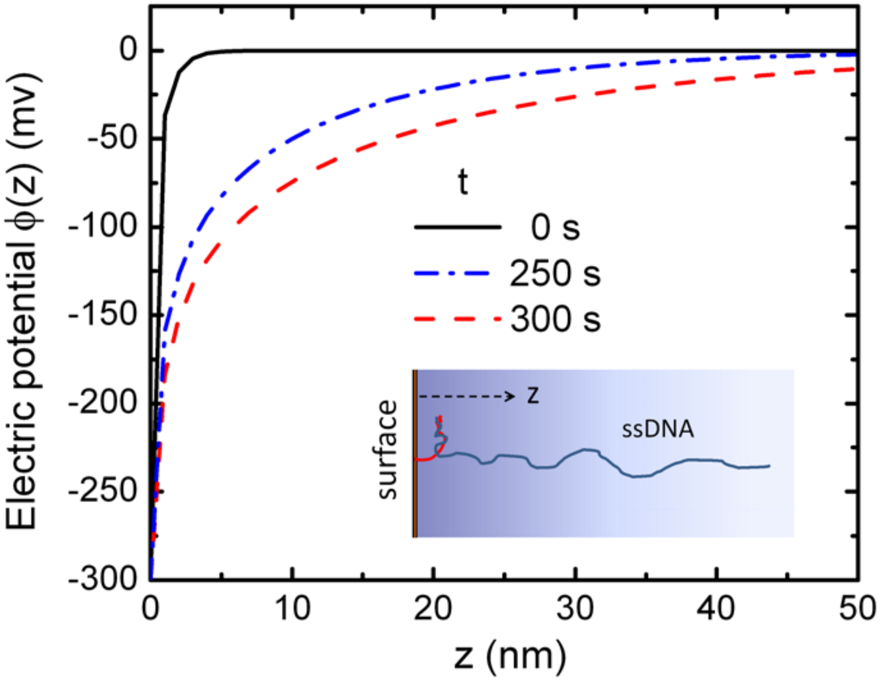

Figure 17. Calculated electric potential distribution along surface normal direction at three representative time point t = 0, 250 and 300 seconds based on electric double layer model system. The inset sketches the model system.

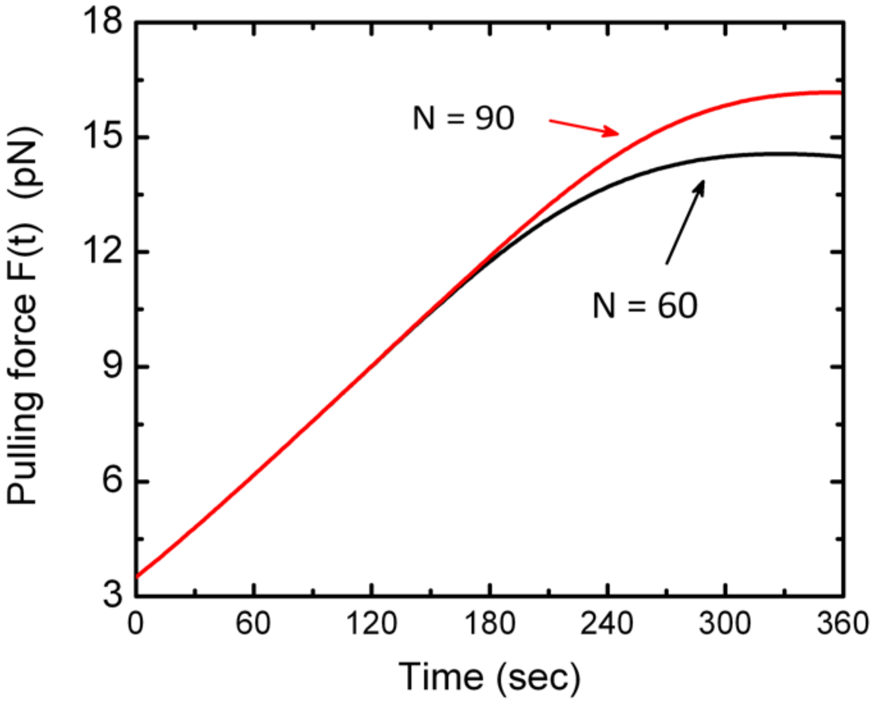

Figure 18. Calculated pulling forces on 60-mer and 90-mer ssDNAs versus time.

4.6 CONCLUSIONS

To conclude, we have developed a novel experimental procedure to separate ssDNAs according to the chain length. We demonstrated that by tethering ssDNA to a gold electrode and applying a relatively low electrode potential to the Au electrode and then gradually decreasing the ion concentration near the electrode, we can detach the tethered short ssDNA chains sequentially. The pulling force is different for ssDNA chains with different chain lengths, and thus with a careful design of the surface potential and the tethering detail, we are able to detach the longer ssDNA chains first and then the shorter ones. We have developed a simple analytical model to understand the experimental mechanism. With reasonable model parameters, the simple electric double layer model provides a semi-quantitative explanation of the experimental results.

5.0 MULTISTAGE MAGNETIC SEPARATION OF MICROSPHERES ENABLED BY TEMPERATURE-RESPONSIVE POLYMERS

5.1 INTRODUCTION

Magnetic separation provides a rapid and simple method for efficient and reliable separation of cells.[147-152] It utilizes magnetic particles to attach to specific cells and separate them from a heterogeneous mixture upon applying an external magnetic field. Typically, the magnetic particles are functionalized with a receptor, which captures the cells selectively, and high separation efficiency is enabled by the extremely high binding affinity and specificity of the receptor, such as an antibody, immobilized on the magnetic particles. However, a major obstacle that prevents the magnetic separation technology from achieving adequate separation efficiencies is non-specific interactions between the cells and magnetic particles. For example, in magnetic cell separation processes that require very large enrichment factors, although the binding affinity of antibodies with the antigen is orders of magnitude greater than the non-specific binding, the effect of non-specific interactions becomes significant and eventually becomes a major challenge.[153-155]

To circumvent the challenge caused by non-specific interactions in current single-stage magnetic separation techniques, we here present a multi-stage separation scheme that is able to yield high enrichment factors by introducing multiple capture-and-release cycles to the magnetic separation process. Poly (N-isopropylacrylamide) (PNIPAM) is the key molecule employed in this work to enable the reversible capture-and-release cycles using magnetic particles. PNIPAM is a stimuli-responsive polymer that exhibits a well-known temperature-responsive phase transition in aqueous solution at 32°C, a lower critical solution temperature (LCST).[156-158] It is hydrophilic assuming a random coil conformation when the temperature is below its LCST in water, but becomes hydrophobic and aggregated with collapsed globule conformation in aqueous solutions when the temperature is above LCST. This reversible temperature responsive phase transition has been utilized for the separation and purification of cells,[159-161] proteins,[162-164] nucleic acids,[165, 166] and other biomolecules.[167] In the present study, the multiple capture-and-release cycles are enabled by attaching PNIPAM to both the magnetic nanoparticles (MNPs) and the targets and manipulating the reversible hydrophobic interactions between such functionalized MNPs and targets. Through temperature cycling, which triggers the reversible hydrophobic-to-hydrophilic phase transition of PNIPAM, we demonstrate that PNIPAM functionalized polystyrene (PS) microspheres can be separated from bare (non-functionalized) PS microspheres in multiple separation stages, and the enrichment factor significantly increases with the number of separation stages. The result indicates that the multi-stage separation scheme can effectively circumvent problems caused by non-specific interactions and significantly improve separation efficiencies of magnetic separation technologies.

5.2 DESIGN OF MULTISTAGE SEPARATION PROCESS

Figure 19 schematically shows the multistage separation process. As a proof of demonstration, PNIPAM-functionalized fluorescent PS microspheres are used as the targets and bare carboxylated PS microspheres (with no PNIPAM) are used as the non-targets. It should be noted that in practical separation processes, the PNIPAM may be conjugated to a bioreceptor such as an antibody and thus attached to the target through antibody-antigen interactions. To capture the PNIPAM-functionalized target PS microspheres by using MNPs, the surface of the MNPs is also grafted with PNIPAM. PNIPAM is a stimuli-responsive polymer that undergoes a reversible coil-to-globule phase transition in dilute aqueous solutions upon changing of the temperature. It is hydrophilic assuming a random coil conformation when the temperature is below its lower critical solution temperature (LCST) (~32°C) in water, but becomes hydrophobic and aggregated with collapsed globule conformation in aqueous solutions when the temperature is above LCST.[156-158] Surface functionalization of MNPs with PNIPAM enables us to reversibly regulate the hydrophobicity of the particle surface by simply cycling the temperature below and above the LCST.

The separation process starts with adding PNIPAM-functionalized MNPs to a mixture of both PNIPAM-functionalized PS microspheres and bare PS microspheres (Figure 19a). Upon raising the temperature to 37°C (>LCST), the PNIPAM molecules on both the MNPs and the target microspheres undergo a hydrophilic-to-hydrophobic phase transition, and the targets are captured by the MNPs due to the hydrophobic interaction between PNIPAM molecules (Figure 19b). During this process, some of the non-target bare PS microspheres may also be attached to the MNPs due to non-specific interactions. Next, the MNPs are magnetically collected in the form of a pellet, which contains the targets captured by the MNPs as well as the non-targets either attached to the MNPs due to non-specific interactions or embedded into the pellet during the agglomeration of the MNPs (Figure 19c). Then, the pellet is separated from the supernatant and re-suspended in a buffer (Figure 19d).

After this first separation cycle, a mixture of target and non-target microspheres has been separated into two parts: one with a higher percentage of non-target microspheres and the other with a higher percentage of target microspheres than those in the original mixture. The percentage increase of the target microspheres in the second mixture may be characterized by using an enrichment factor, which is defined as the increase (typically in the number of folds) of the ratio of target to non-target microspheres as a result of the separation process. The enrichment factor obtained after one separation cycle is limited by the non-specific interactions between the PNIPAM molecules and the non-targets. The reversible hydrophobic-to-hydrophilic conformational transition of PNIPAM enables us to improve this enrichment factor by repeating this separation process through cycling the temperature. Upon cooling the buffer to 4°C and redispersion, the PNIPAM on both the MNPs and the target PS microspheres is triggered to its hydrophilic conformation, which detaches the target PS microspheres from the MNPs (Figure 19e) and initiates another separation cycle. Repeating this capture-and-release procedure (Figures 19e-19h) multiple times can effectively circumvent problems caused by the non-specific interactions and significantly improve the separation efficiency. It should be noted that for the purpose of demonstration, our interest in this experiment is to increase the percentage of the target microspheres in the target-rich mixture as we repeat the separation cycle, but the same mechanism is also applicable to increasing the percentage of the non-target microspheres.

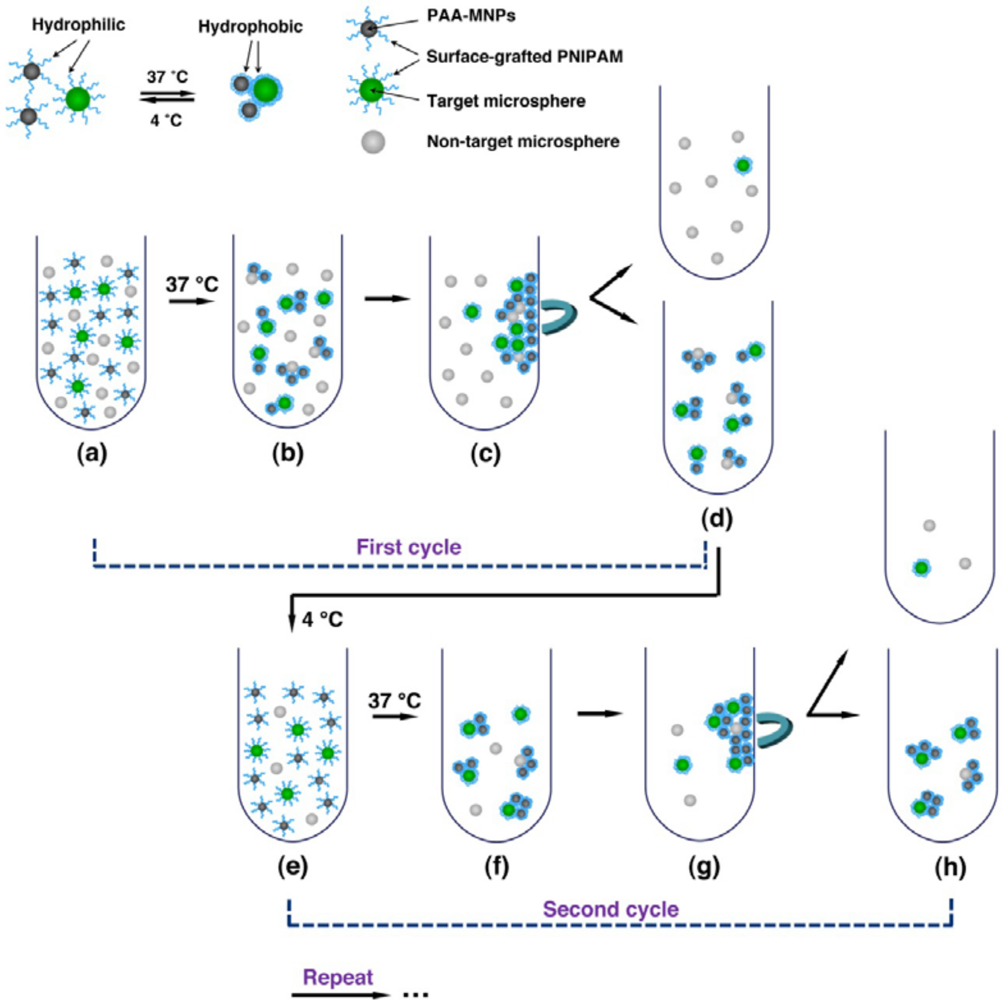

Figure 19. Schematic of the multistage magnetic separation process using PNIPAM functionalized magnetic nanoparticles (PNIPAM-MNPs). (a) PNIPAM-MNPs, target microspheres, and non-target microspheres are mixed in a 4°C buffer. (b) Capture of the targets by PNIPAM-MNPs through hydrophobic interactions upon raising the temperature to 37°C. (c) The MNPs are collected by a magnet. (d) The original mixture is separated into two parts: the pellet contains MNPs, the captured targets, and the non-targets captured due to non-specific interactions; the supernatant contains the rest of the mixture and is decanted. (e) Release of the targets from PNIPAM-MNPs in a 4°C buffer. (f) - (h) repeat the process of (b) - (d).

5.3 MATERIALS AND METHODS

5.3.1 Materials

Nonfluorescent 4.95 μm carboxylated polystyrene microspheres and 5.78 μm green fluorescent carboxylated polystyrene (PS) microspheres with an excitation wavelength of 480 nm and an emission wavelength of 520 nm were obtained from Bangs Laboratories, Inc. The surface density of carboxyl groups on the fluorescent PS microspheres is about 1.075×10^{18} COOH/m^2. Ethylene glycol was purchased from J.T. Baker. Amino terminated poly (Nisopropylacrylamide) (PNIPAM) (Mn = 45,600 g/mol, PDI = 1.62) were purchased from Polymer Source, Inc. and used as received. Iron (III) chloride ($FeCl_3$), ethanolamine, sodium acetate (NaAc), poly(acrylic acid) (PAA, Mw~2000 g/mol), 1-ethyl-3-(3 dimethylaminopropyl) carbodiimide hydrochloride (EDC), 2-(N-morpholino)ethanesulfonic acid (MES) and bovine serum albumin (BSA) were purchased from Sigma-Aldrich. All buffers were prepared or diluted in deionized water.

5.3.2 Synthesis of poly(acrylic acid)-modified Fe_3O_4 magnetic nanoparticles (PAA-MNPs)

PAA-MNPs were synthesized by using a solvothermal method. Briefly, $FeCl_3$ (0.8 g) was dissolved in ethylene glycol (40 ml) with vigorous stirring, followed by addition of NaAc (3.6 g) and PAA (1.0 g). The mixture was stirred continuously for 30 min, sealed in a teflon-lined stainless-steel autoclave, and then reacted at 200 °C for 10 h. After the reaction was finished, the autoclave was cooled to room temperature. The products were collected, washed several times with ethanol, and then dried under vacuum at 60 °C before characterization and usage.

5.3.3 Characterization of PAA-MNPs

The size and morphology of the as-synthesized PAA-MNPs were characterized using scanning electron microscopy (SEM, Philips XL-30 field, 15 kV). The crystal structures of the PAA-MNPs were examined by using powder X-ray diffraction (XRD) (Philips X’pert Diffractometer using CuKα radiation, λ=1.54178 Å). The chemical composition of the PAA-MNPs was examined by Fourier transform infrared (FT-IR) spectrometry. The sample of PAA-MNPs was washed five times with ethanol, redispersed in water and dried in a powder form. FTIR samples were prepared using a KBr-pellet method, and the spectra were collected by a Bruker Vertex-70LS FT-IR spectrometer.

5.3.4 Conjugation of PAA-MNPs and green fluorescent carboxylated PS microspheres with PNIPAM

The carboxyl group on the surfaces of PAA-MNPs and green fluorescent PS microspheres was used to covalently link amino-terminated PNIPAM to the surfaces by using 1-ethyl-3-(3-dimethylaminopropyl) carbodiimide hydrochloride (EDC) chemistry. The PAA-MNPs (0.5 ml, 2.5%) were washed three times in 0.1 M carbonate buffer (pH 9.6) and then another three times in 0.1 M MES buffer (pH 6.5). After washing, the MNPs were redispersed in MES buffer. To activate the carboxyl groups, fresh solution of EDC (2%, w/v) in MES buffer was added and the mixture was incubated for 3 h at room temperature in the dark. After incubation, the MNPs were washed three times with MES buffer to remove the unreacted EDC. Then, the MNPs were redispersed in 0.1 M borate buffer (pH 8.5) and enough amount of amino terminated PNIPAM was added for the functionalization. The mixture was incubated overnight at room temperature in the dark. Following conjugation, the MNPs were magnetically separated and thoroughly washed with PBS (pH 7.4) to remove unbound amino-terminated PNIPAM, and then incubated in the blocking solution (0.3 M ethanolamine in borate buffer) for 30 min to block the unreacted carboxylate sites. The MNPs were then rinsed thoroughly, and finally stored in storage buffer (PBS, 0.1% BSA w/v) with a concentration of 1 mg/mL at 4°C. Similar procedure was used for grafting of amino-terminated PNIPAM to green fluorescent carboxylated PS microspheres.

5.3.5 Reversible capture-and-release of target microspheres using PNIPAM-MNPs

Specified amount of PNIPAM-MNPs was added into a sample of PNIPAM-functionalized green fluorescent microspheres suspended in 1 mL 4°C PBS buffer. The mixture was warmed up to 37°C and then incubated for 10 min in the dark. The aggregates were then collected by a neodymium-iron-boron magnet. The magnetically collected microspheres were separated from the supernatant and then redispersed in a 4°C PBS buffer. As a comparison, bare PS microspheres were used in the capture-and-release cycles in the same manner.

5.3.6 Multistage separation of microspheres through reversible capture-and-release cycles

PNIPAM-functionalized green fluorescent microspheres were used as target microspheres, while carboxylated bare non-fluorescent polystyrene microspheres were used as non-target microspheres. Mixtures of target and non-target microspheres at four different ratios of $1:10^2$, $1:10^3$, $1:10^4$ and $1:10^5$, respectively, were used in the experiments. The separation process started with adding a certain amount of PNIPAM-MNPs to the mixture containing both the target and the non-target microspheres. The mixture was then incubated at 37°C for 10 min in the dark. After incubation, a magnet was used to pull the MNPs and PS microspheres attached to the MNPs out of the mixture. The magnetically collected particles were then separated from the supernatant, re-suspended in the PBS, and incubated for 10 min at 4°C in the dark. The above capture-and-release cycle was repeated for a specified number of times.

5.3.7 Counting of PS microspheres

PS microspheres were counted and the numbers of bare (nonfluorescent) and fluorescent PS microspheres in PBS buffer after each capture-and-release cycle were determined using a BD FACSAria flow cytometer (BD BioSciences, San Jose, CA).

5.4 RESULTS AND DISCUSSION

The PAA-MNPs were synthesized by a one-step solvothermal method, where PAA in the reaction system acted both as a ligand and a surface functionalization agent. Figure 20a presents an SEM image of the resulting products. It can be seen that the as-synthesized PAA-MNPs are spheres of about 300 nm in diameter with a narrow size distribution. Figure 20b presents the XRD pattern of the product, which can be indexed to Fe_3O_4 (JCPDS 75-1609). The PAA-MNPs were easily dispersed in water by sonication and the dispersion remained stable for more than 0.5 h before precipitation occurred. Upon placement of a magnet next to the vial, the PAA-MNPs were quickly attracted to the magnet and agglomerated at the vial wall within a few seconds, leaving the supernatant transparent (Figure 20c). After removing the magnet, the PAA-MNPs were easily redispersed in water with gentle shaking (Figure 20d). Figure 20e compares the FT-IR spectra of pure PAA and PAA-MNPs. Both spectra show bands at 1730 cm^{-1}, 1450 cm^{-1}, 1413 cm^{-1} and 1560 cm^{-1}, which are characteristics of the PAA—the band at 1730 cm^{-1} is characteristic of the C=O stretching mode for the protonated carboxylate group, and the other 3 bands are associated with the CH_2 bending mode, symmetric and asymmetric C-O stretching modes of the COO^- group, respectively.[168-170] These results indicate the presence of PAA on the surface of the MNPs even after extensive washing. The carboxyl groups on the surface of PAA-MNPs were used to covalently attach amino-terminated PNIPAM to the MNPs, which were employed to separate PNIPAM-functionalized microspheres from bare microspheres in the subsequent experiments.

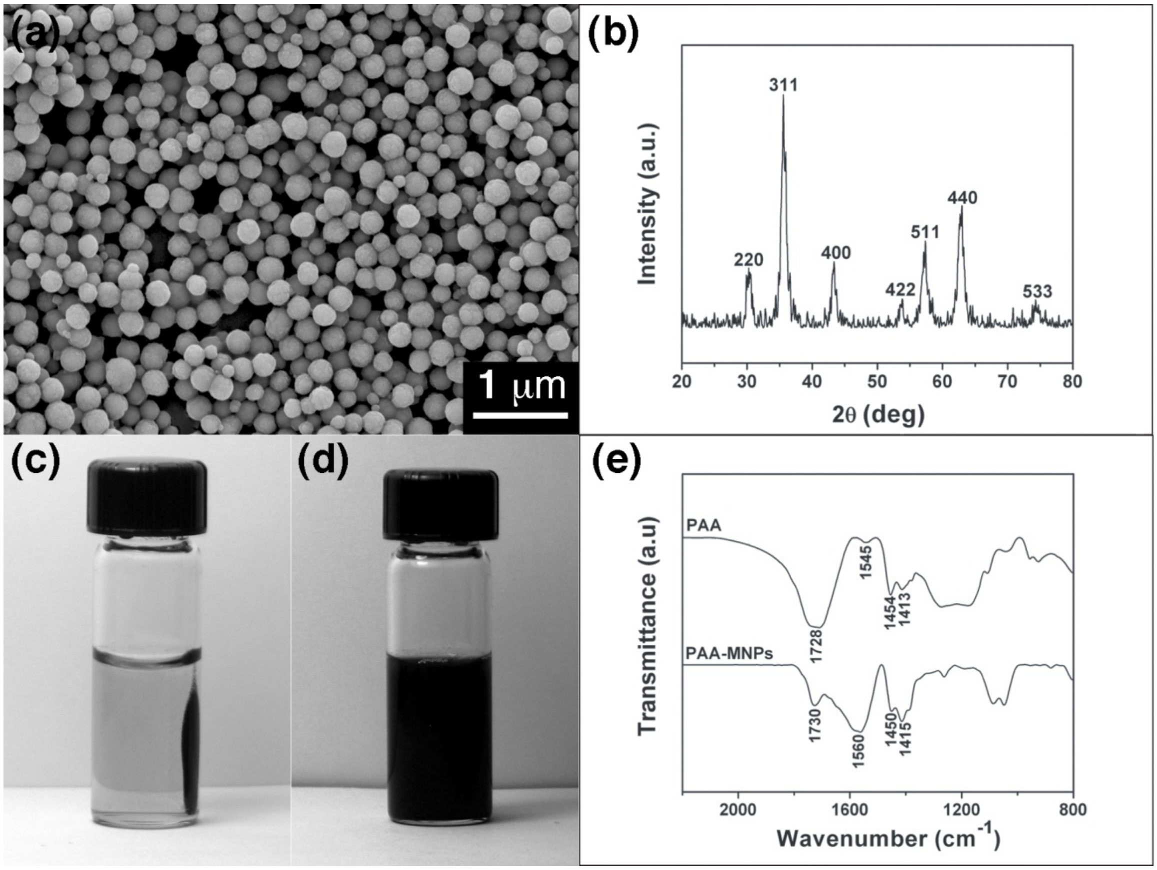

Figure 20. Characterizations of poly (acrylic acid) modified magnetic nanoparticles (PAA-MNPs). (a) SEM image. (b) XRD pattern. (c) Magnetic property of the PAA-MNPs: the MNPs are attracted to the wall of the vial when a magnet is present. (d) After removing the magnet, the PAA-MNPs are easily redispersed in water with gentle shaking. (e) FTIR spectra of PAA and PAA-MNPs.

We first examined the effect of the concentration of PNIPAM-MNPs on the capture efficiency of PNIPAM-functionalized target microspheres. In this set of experiments, PNIPAM-functionalized target microspheres were mixed with PNIPAM-MNPs in different concentrations. The final concentration of PNIPAM-functionalized microspheres in all samples was 5.0×10^6 microspheres/mL and the concentration of PNIPAM-MNPs was varied from 0.005 to 0.12 mg/ml. A capture-and-release cycle was carried out as described in the experimental design. The steps were the same as those shown in Figures 19a-19e except that the mixture did not contain non-target microspheres in this set of experiments. The capture efficiency was determined by measuring the percentage of the target microspheres left in the mixture after the cycle. Figure 21 plots the capture efficiency as a function of the concentration of PNIPAM-MNPs employed at the start of the process. It is observed that the capture efficiency increases from ~22% to ~ 92% when the concentration of the PNIPAM-MNPs is increased from 0.005 to 0.03 mg/mL, after which a plateau occurs—further increase of the PNIPAM-MNP concentration does not significantly affect the capture efficiency of target microspheres. This indicates that for a certain concentration of target microspheres, the concentration of MNPs is not critical as long as enough MNPs are used. For multiple capture-and-release cycles, this implies that if enough MNPs are used for the first separation cycle, the concentration of MNPs does not need to be adjusted for subsequent separation cycles as the total number of target microspheres slightly decreases due to the less than unity capture efficiencies. For the subsequent experiments conducted in this work, the concentration of target microspheres was kept at 5.0×10^6 microspheres/mL or less and, therefore, 0.05 mg/mL PNIPAM-MNPs was used in the separation processes.

We next examined the selectivity of one capture-and-release cycle by comparing the number of PNIPAM-functionalized target microspheres with that of the non-target carboxyl-terminated microspheres captured and released in the process. For such comparison, we started with two mixtures made by adding the same amount of PNIPAM-MNPs to suspensions of target microspheres and non-target microspheres, respectively. In both mixtures, the final concentration of the microspheres was about 5.0×10^6 microspheres/mL and the concentration of the PNIPAM-MNPs was 0.05 mg/mL. After raising the temperature and magnetically collecting the MNPs (as schematically shown in Figures 19a-19d), the PS microspheres in the supernatant (Figure 19d) of each mixture were counted and the percentage of PS microspheres captured by the MNPs in the pellet was calculated. Afterwards, the pellet was re-dispersed in 4ºC buffer, and the PS microspheres released from the MNP in the buffer were counted. Figure 22 presents the percentages of the target PS microspheres captured and released by the MNP in comparison to those of the non-target PS microspheres. The data are based on five independent experiments. In average, about 92% of the target microspheres were captured by the MNPs, and about 91% of the target microspheres were released after the capture in one capture-and-release cycle. In comparison, only less than 5% of the non-target microspheres were left in the mixture after one capture-and-release cycle.

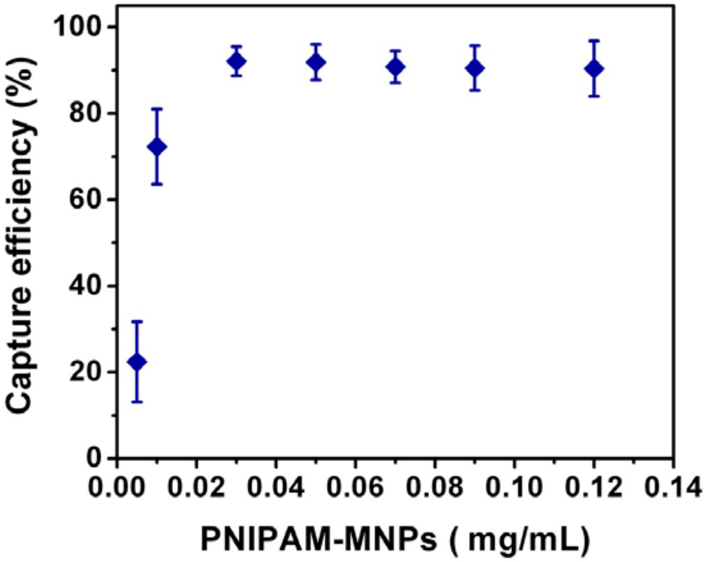

Figure 21. Effect of the concentration of PNIPAM-MNPs on the capture efficiency of the target microspheres. The initial concentration of target microspheres is 5.0×10^6 microspheres/mL. For each sample, one capture-and-release cycle is performed. Data are presented as the mean and standard deviation from five independent experiments.

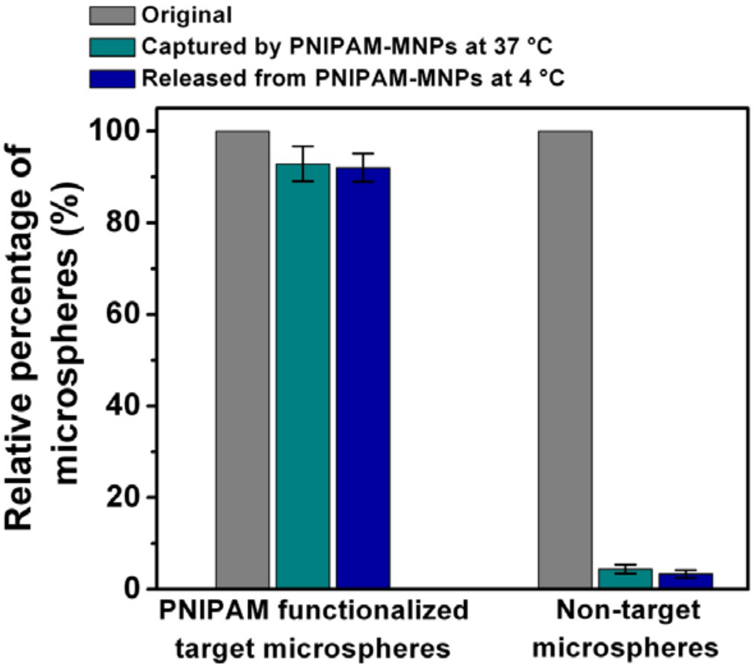

Figure 22. Comparative study on the capture-and-release specificity of PNIPAM-functionalized target microspheres and non-target microspheres (bare PS microspheres) using PNIPAM-MNPs. The initial concentrations of target and non-target microspheres are 5.0×10^6 and 4.9×10^6 microspheres/mL, respectively. The percentages of microspheres counted after each capture or release process are presented using the number of microspheres in the original sample as a reference. The average and standard deviation are calculated from five independent data sets.

The large difference between the percentages of target and non-target PS microspheres left in the mixture after one capture-and-release cycle and the capability of reversibly tuning the hydrophobicity of the PNIPAM molecule on both the target PS microspheres and the MNPs enable us to develop a multistage separation technique by repeating the capture-and-release cycles. To demonstrate the capability of such a technique, we mixed target microspheres with non-target microspheres at various ratios of $1:10^2$, $1:10^3$, $1:10^4$ and $1:10^5$, and a specified number of separation cycles were carried out with each sample. The overall enrichment factors k_{overall} (defined as the increase, in the number of folds, of the ratio of target to non-target microspheres as a result of the separation cycles) obtained with each sample after up to 5 capture-and-release cycles are presented in Figure 23. It is evident that the overall enrichment factors significantly increase with the number of capture-and-release cycles. For example, one capture-and-release cycle was able to increase the ratio of the target to non-target microspheres ($R_{\mathrm{T/NT}}$) from initially $1{:}10^2$ (or 0.01) to 0.133; 3 capture-and-release cycles were able to increase it to 14.05; and 5 cycles were able to increase it to 2,100. Correspondingly, the enrichment factors were 13.3, 1,405, and 2.10×10^4 after one, three, and five capture-and-release cycles, respectively. The significance of multiple separation cycles becomes more apparent when the initial $R_{\mathrm{T/NT}}$ decreases. For example, overall enrichment factors of 1.21×10^5, 1.69×10^5, and 1.87×10^5 were obtained when the initial $R_{\mathrm{T/NT}}$ was $1{:}10^3$, $1{:}10^4$, and $1{:}10^5$, respectively. Figure 6 plots the single cycle enrichment factor $k_{\text{single-cycle}}$ versus $R_{\mathrm{T/NT}}$ for each cycle based on the data obtained from all four samples. The $k_{\text{single-cycle}}$ appears to decrease as $R_{\mathrm{T/NT}}$ increases, which implies that further enriching the target microspheres becomes more difficult as their concentration increases. Therefore, smaller overall enrichment factors are expected as the initial $R_{\mathrm{T/NT}}$ increases.

The above experiments demonstrate the feasibility of the multistage separation scheme. For demonstration purposes, the temperature-responsive molecule used in our experiment is PNIPAM and it is covalently attached to the target PS microspheres. In practical applications, selective attaching of PNIPAM to the targets may be realized by linking the PNIPAM molecule to an antibody,[171] which selectively captures the targets and therefore attaches the PNIPAM molecule to their surface. Besides PNIPAM, a family of temperature-responsive molecules may function in the same manner.[172, 173] In addition, other biopolymers, such as elastin-like polypeptides (ELPs), are also able to undergo a reversible phase transition from water soluble forms into hydrophobic aggregates over a wide range of temperature and pH.[174-176] Such polypeptides may be fused to antibodies through protein engineering.[177-179] In particular, functional ELP fusions with ProA, ProG or ProL are able to conjugate with a wide range of antibodies,[180-182] and thus may be used in our multistage separation processes. It is worth noting that the PS microspheres used in our experiment have similar size as cells and, therefore, our result implies that the separation method presented here may be applicable to separation and purification of cells.

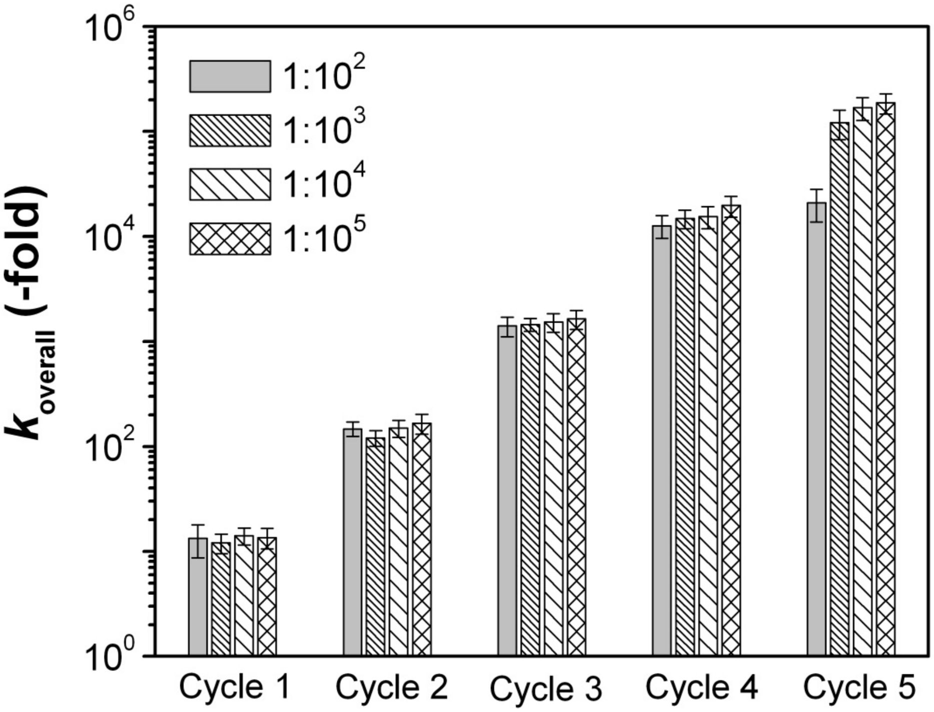

Figure 23. Overall enrichment factor $k_{overall}$ as a function of the separation cycles for mixtures with various initial ratios of target to non-target microspheres. The mean and standard deviation are calculated from five independent data sets.

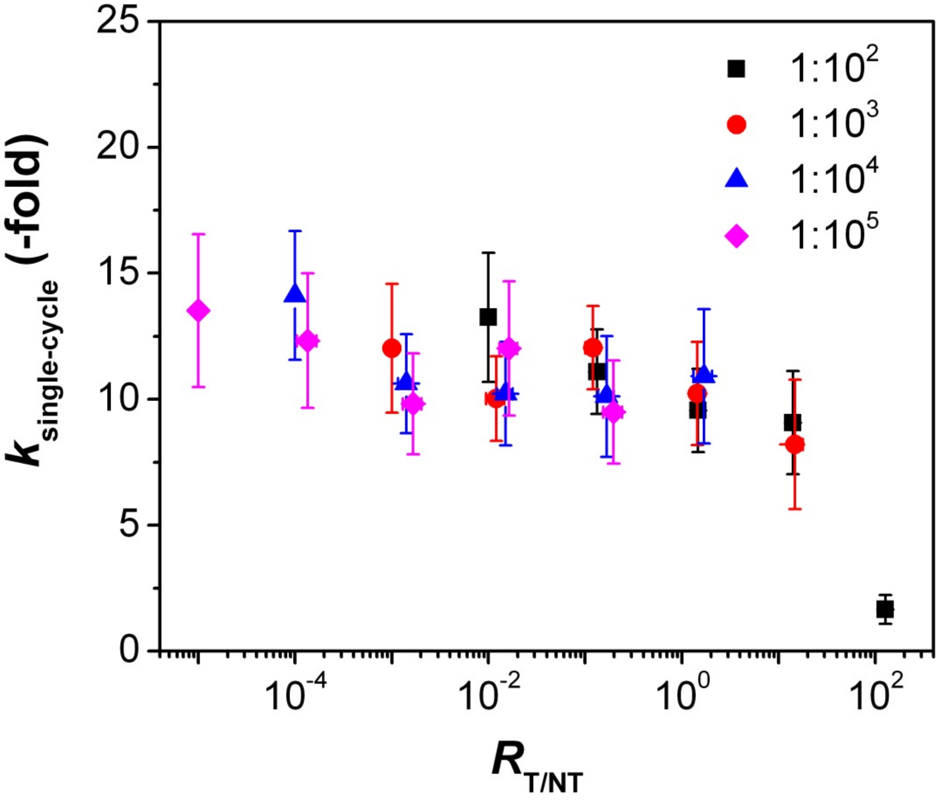

Figure 24. Single-cycle enrichment factor $k_{single\text{-}cycle}$ versus the ratio of target to non-target microspheres ($R_{\text{T/NT}}$) before each cycle calculated for samples with 4 different initial $R_{\text{T/NT}}$ values. The mean and standard deviation are calculated from five independent data sets.

5.5 CONCLUSIONS

We have demonstrated a multistage magnetic separation process that is able to separate PNIPAM-functionalized PS microspheres from bare PS microspheres by using PNIPAM-functionalized MNPs. The reversible hydrophilic-to-hydrophobic transition of PNIPAM molecules enables us to manipulate the hydrophobic interactions between the MNPs and the microspheres upon cycling the temperature, and to separate the target microspheres from non-target microspheres in multiple stages through capture-and-release cycles. The overall enrichment factor is observed to significantly increase with the number of separation stages, and reaches as high as 1.87×10^5 after 5 stages. The result implies that such a multistage separation scheme may effectively circumvent problems caused by the non-specific interactions in magnetic separation processes.

6.0 SUMMARY

This dissertation consists of two main parts. In the first part, we have developed a novel DNA separation technology that is more efficient than the conventional electrophoresis-based technologies. Our strategy is to immobilize DNA molecules on a solid surface through precise end-hybridization and sequentially pull the DNA molecules off the surface with increasing electric field. The anchor is such designed that the critical force to detach a DNA fragment is independent of the chain length. Because the electrical force applied to each DNA fragment is proportional to its net charge, a gradual increase of the electric field leads to a size-based detachment of the DNA strands-longer DNA fragments first departing the surface followed by the shorter ones. We have been able to use this method to separate long DNA molecules by length, such as the efficient separation of lambda dsDNA (48,502 bp) from human genomic dsDNA (> 100,000 bp), with the application of a DC electric field in a simple sandwich-like chamber. This simple and highly efficient separation technology does not require separation matrices such as gels or polymer solutions, and in principle has no upper limit on the length of the DNA that can be efficiently separated.

We were able to extend this separation strategy to the separation of short single-stranded (ss) DNA fragments with less than 100 nucleotides (nt). To pull the short ssDNA fragments off the surface, a very strong electric field (on the order of 10^5 V/m) should be applied to produce large enough stretching force on the ssDNA. Using the original experimental set-up for long

DNA separation may cause various technical problems such as Joule heating and side electrochemical reactions due to the large electric current. We developed two approaches to overcome these problems. The first approach is employing a microfluidic platform with narrow channels filled with a low conductivity buffer. The electric current in the buffer was lowered to less than a few microamperes even at the highest electric field strength, and the influence of Joule heating can be safely neglected. We are able to separate ssDNA fragments in four different lengths (60nt, 70nt, 80nt and 90nt) with a 10-nt resolution using this integrated microfluidic platform. Theoretical analysis indicates that the separation resolution is limited by the fluctuation forces on tethered DNA chains, which agrees well with experimental results.

In the second approach, we were able to separate short ssDNA fragments by taking the advantage of the strong yet evolving non-uniform electric field near the Au surface in contact with a buffer solution that is gradually diluted by deionized water. The high electric field strength inside the electrical double layer at the gold/electrolyte interface allows us to pull short ssDNA strands off the surface with a very low electrode potential. Electrochemical reactions are avoided by maintaining the low electrode potential within the ideally polarizable region. Tuning the ion concentration of the electrolyte solution allows regulation of the non-uniform electric field. By gradually decreasing the ion concentration, longer ssDNA strands are detached first and then followed by the shorter ones. A numerical analysis based on a simple electric double layer model provides semi-quantitative explanations of the experimental results.

In the second part of this dissertation, we developed a multistage separation strategy that is able to effectively circumvent the problem caused by the non-specific interactions by introducing multiple capture-and-release cycles to the magnetic separation process. We have demonstrated a multistage magnetic separation process that is able to separate PNIPAM-functionalized PS microspheres from bare PS microspheres by using PNIPAM-functionalized MNPs. The reversible hydrophilic-to-hydrophobic transition of PNIPAM molecules enables us to manipulate the hydrophobic interactions between the MNPs and the microspheres upon cycling the temperature, and to separate the target microspheres from non-target microspheres in multiple stages through capture-and-release cycles. The overall enrichment factor is observed to significantly increase with the number of separation stages, and reaches as high as 1.87×10^5 after 5 stages. For demonstration purposes, the temperature-responsive molecule used in our experiment is PNIPAM and it is covalently attached to the target PS microspheres. For practical applications, selective attaching of PNIPAM to the targets may be realized by linking the PNIPAM molecule to an antibody, which selectively captures the targets and therefore attaches the PNIPAM molecule to their surface. In addition, other biopolymers, such as elastin-like polypeptides (ELPs), are also able to undergo a reversible phase transition from hydrophilic forms into hydrophobic aggregates over a wide range of temperature and pH. Such polypeptides may be fused to antibodies through protein engineering. In particular, functional ELP fusions with ProA, ProG or ProL are able to conjugate with a wide range of antibodies, and thus may be used in the multistage separation processes for the separation of biological type samples.

BIBLIOGRAPHY

1. DeDionisio, L.A. and D.H. Lloyd, *Capillary gel electrophoresis and antisense therapeutics analysis of DNA analogs.* Journal of Chromatography A, 1996. **735**(1-2): p. 191-208.

2. Srivatsa, G.S., et al., *Quantitative capillary gel electrophoresis assay of phosphorothioate oligonucleotides in pharmaceutical formulations.* Journal of Chromatography A, 1994. **680**(2): p. 469-477.

3. Slater, G., C. Desruisseaux, and S. Hubert, *DNA Separation Mechanisms During Electrophoresis*, in *Capillary Electrophoresis of Nucleic Acids*, K. Mitchelson and J. Cheng, Editors. 2001, Humana Press. p. 27-41.

4. Lerman, L.S. and H.L. Frisch, *Why does the electrophoretic mobility of dna in gels vary with the length of the molecule.* Biopolymers, 1982. **21**(5): p. 995-997.

5. Viovy, J.L., *Electrophoresis of DNA and other polyelectrolytes: Physical mechanisms.* Reviews of Modern Physics, 2000. **72**(3): p. 813-872.

6. Sartori, A., V. Barbier, and J.L. Viovy, *Sieving mechanisms in polymeric matrices.* Electrophoresis, 2003. **24**(3): p. 421-440.

7. Caetanoanolles, G., B.J. Bassam, and P.M. Gresshoff, *DNA amplification fingerprinting using very short arbitrary oligonucleotide primers.* Bio-Technology, 1991. **9**(6): p. 553-557.

8. Maniatis, T., A. Jeffrey, and H. Vandesande, *Chain-length determination of small double-stranded and single-stranded-dna molecules by polyacrylamide-gel electrophoresis.* Biochemistry, 1975. **14**(17): p. 3787-3794.

9. Johansso.Bg, *Agarose-gel electrophoresis.* Scandinavian Journal of Clinical & Laboratory Investigation, 1972. **29**: p. 7-19.

10. Smisek, D.L. and D.A. Hoagland, *Agarose gel electrophoresis of high molecular weight, synthetic polyelectrolytes.* Macromolecules, 1989. **22**(5): p. 2270-2277.

11. Heller, C. and F.M. Pohl, *A systematic study of field inversion gel electrophoresis.* Nucleic Acids Res, 1989. **17**(15): p. 5989-6003.

12. Hatano, S., J. Yamaguchi, and A. Hirai, *The preparation of high-molecular-weight DNA from rice and its analysis by pulsed-field gel electrophoresis.* Plant Science, 1992. **83**(1): p. 55-64.

13. Levene, S.D., *Theories of Pulsed-Field Gel Electrophoresis*, 1992. p. 347-365.

14. Gunderson, K. and G. Chu, *Pulsed-field electrophoresis of megabase-sized DNA.* Molecular and Cellular Biology, 1991. **11**(6): p. 3348-3354.

15. Chu, G., *Pulsed field electrophoresis in contour-clamped homogeneous electric-fields for the resolution of dna by size or topology.* Electrophoresis, 1989. **10**(5-6): p. 290-295.

16. Schwartz, D.C. and C.R. Cantor, *Separation of yeast chromosome-sized DNAs by pulsed field gradient gel electrophoresis.* Cell, 1984. **37**(1): p. 67-75.

17. Shaw, D.J., *Separation of Large DNA Molecules by Pulsed-Field Gel Electrophoresis #*, in *T Protocols in Molecular Neurobiology*1992. p. 1-13.

18. Birren, B.W., et al., *Optimized Conditions For Pulsed Field Gel-Electrophoretic Separations Of DNA.* Nucleic Acids Research, 1988. **16**(15): p. 7563-7582.

19. Jorgenson, J.W. and K.D. Lukacs, *Zone electrophoresis in open-tubular glass-capillaries.* Analytical Chemistry, 1981. **53**(8): p. 1298-1302.

20. Jorgenson, J.W. and K.D. Lukacs, *Capillary zone electrophoresis.* Science, 1983. **222**(4621): p. 266-272.

21. Gordon, M.J., et al., *Capillary electrophoresis.* Science, 1988. **242**(4876): p. 224-228.

22. Guttman, A. and N. Cooke, *Capillary gel affinity electrophoresis of DNA fragments.* Analytical Chemistry, 1991. **63**(18): p. 2038-2042.

23. Woolley, A.T. and R.A. Mathies, *Ultra-high-speed dna fragment separations using microfabricated capillary array electrophoresis chips.* Proceedings of the National Academy of Sciences of the United States of America, 1994. **91**(24): p. 11348-11352.

24. Grossman, P.D. and D.S. Soane, *Experimental and theoretical-studies of dna separations by capillary electrophoresis in entangled polymer-solutions.* Biopolymers, 1991. **31**(10): p. 1221-1228.

25. Kleemiss, M.H., M. Gilges, and G. Schomburg, *Capillary electrophoresis of dna restriction fragments with solutions of entangled polymers.* Electrophoresis, 1993. **14**(5-6): p. 515-522.

26. Grossman, P.D. and D.S. Soane, *Capillary electrophoresis of dna in entangled polymer-solutions.* Journal of Chromatography, 1991. **559**(1-2): p. 257-266.

27. Bashkin, J.S., et al., *Implementation of a capillary array electrophoresis instrument.* Journal of Capillary Electrophoresis, 1996. **3**(2): p. 61-68.

28. Emrich, C.A., et al., *Microfabricated 384-lane capillary array electrophoresis bioanalyzer for ultrahigh-throughput genetic analysis.* Anal Chem, 2002. **74**(19): p. 5076-5083.

29. Marsh, M., et al., *High-throughput DNA sequencing on a capillary array electrophoresis system.* Journal of Capillary Electrophoresis, 1997. **4**(2): p. 83-89.

30. Slater, G.W., et al., *The theory of DNA separation by capillary electrophoresis.* Current Opinion in Biotechnology, 2003. **14**(1): p. 58-64.

31. Bruin, G.J.M., et al., *Capillary zone electrophoretic separations of proteins in polyethylene glycol-modified capillaries.* Journal of Chromatography, 1989. **471**: p. 429-436.

32. Engelhardt, H. and M.A. Cunatwalter, *Preparation and stability-tests for polyacrylamide-coated capillaries for capillary electrophoresis.* Journal of Chromatography A, 1995. **716**(1-2): p. 27-33.

33. Kohr, J. and H. Engelhardt, *Capillary electrophoresis with surface coated capillaries.* Journal of Microcolumn Separations, 1991. **3**(6): p. 491-495.

34. Magnusdottir, S., et al., *Electrohydrodynamically induced aggregation during constant and pulsed field capillary electrophoresis of DNA.* Biopolymers, 1999. **49**(5): p. 385-401.

35. Mitnik, L., et al., *Segregation in DNA solutions induced by electric fields.* Science, 1995. **267**(5195): p. 219-222.

36. Volkmuth, W.D. and R.H. Austin, *DNA electrophoresis in microlithographic arrays.* Nature, 1992. **358**(6387): p. 600-602.

37. Jacobson, S.C. and J.M. Ramsey, *Integrated microdevice for DNA restriction fragment analysis.* Analytical Chemistry, 1996. **68**(5): p. 720-723.

38. Duke, T.A.J. and R.H. Austin, *Microfabricated sieve for the continuous sorting of macromolecules.* Physical Review Letters, 1998. **80**(7): p. 1552-1555.

39. Turner, S.W., et al., *Monolithic nanofluid sieving structures for DNA manipulation.* Journal of Vacuum Science & Technology B, 1998. **16**(6): p. 3835-3840.

40. Chou, C.F., et al., *Sorting by diffusion: An asymmetric obstacle course for continuous molecular separation.* Proceedings of the National Academy of Sciences of the United States of America, 1999. **96**(24): p. 13762-13765.

41. Kaji, N., et al., *Separation of long DNA molecules by quartz nanopillar chips under a direct current electric field.* Analytical Chemistry, 2004. **76**(1): p. 15-22.

42. Fu, J.P., et al., *A patterned anisotropic nanofluidic sieving structure for continuous-flow separation of DNA and proteins.* Nature Nanotechnology, 2007. **2**(2): p. 121-128.

43. Han, J., S.W. Turner, and H.G. Craighead, *Entropic trapping and escape of long DNA molecules at submicron size constriction.* Physical Review Letters, 1999. **83**(8): p. 1688-1691.

44. Han, J. and H.G. Craighead, *Separation of long DNA molecules in a microfabricated entropic trap array.* Science, 2000. **288**(5468): p. 1026-1029.

45. Han, J.Y. and H.G. Craighead, *Characterization and optimization of an entropic trap for DNA separation.* Analytical Chemistry, 2002. **74**(2): p. 394-401.

46. Cabodi, M., S.W.P. Turner, and H.G. Craighead, *Entropic Recoil Separation of Long DNA Molecules.* Analytical Chemistry, 2002. **74**(20): p. 5169-5174.

47. Turner, S.W., M. Cabodi, and H.G. Craighead, *Confinement-induced entropic recoil of single DNA molecules in a nanofluidic structure.* Phys Rev Lett, 2002. **88**(12): p. 128103.

48. Doyle, P.S., et al., *Self-assembled magnetic matrices for DNA separation chips.* Science, 2002. **295**(5563): p. 2237-2237.

49. Zeng, Y. and D.J. Harrison, *Self-assembled colloidal arrays as three-dimensional nanofluidic sieves for separation of biomolecules on microchips.* Analytical Chemistry, 2007. **79**(6): p. 2289-2295.

50. Tabuchi, M., et al., *Nanospheres for DNA separation chips.* Nature Biotechnology, 2004. **22**(3): p. 337-340.

51. Minc, N., et al., *Quantitative microfluidic separation of DNA in self-assembled magnetic matrixes.* Analytical Chemistry, 2004. **76**(13): p. 3770-3776.

52. Gijs, M.A.M., *Magnetic bead handling on-chip: new opportunities for analytical applications.* Microfluidics and Nanofluidics, 2004. **1**(1): p. 22-40.

53. Kasianowicz, J.J., et al., *Characterization of individual polynucleotide molecules using a membrane channel.* Proceedings of the National Academy of Sciences of the United States of America, 1996. **93**(24): p. 13770-13773.

54. Bayley, H. and C.R. Martin, *Resistive-Pulse Sensing-From Microbes to Molecules.* Chem Rev, 2000. **100**(7): p. 2575-2594.

55. Chimerel, C., et al., *Transport at the nanoscale: temperature dependence of ion conductance.* Eur Biophys J, 2008. **38**(1): p. 121-125.

56. Danelon, C., et al., *Interaction of zwitterionic penicillins with the OmpF channel facilitates their translocation.* Biophys J, 2006. **90**(5): p. 1617-1627.

57. Chen, P., et al., *Probing single DNA molecule transport using fabricated nanopores.* Nano Letters, 2004. **4**(11): p. 2293-2298.

58. Dekker, C., *Solid-state nanopores.* Nature Nanotechnology, 2007. **2**(4): p. 209-215.

59. Fologea, D., et al., *Slowing DNA translocation in a solid-state nanopore.* Nano Letters, 2005. **5**(9): p. 1734-1737.

60. Howorka, S., S. Cheley, and H. Bayley, *Sequence-specific detection of individual DNA strands using engineered nanopores.* Nature Biotechnology, 2001. **19**(7): p. 636-639.

61. Branton, D., et al., *The potential and challenges of nanopore sequencing.* Nature Biotechnology, 2008. **26**(10): p. 1146-1153.

62. Ibrahim, S.F. and G. van den Engh, *High-speed cell sorting: fundamentals and recent advances.* Current Opinion in Biotechnology, 2003. **14**(1): p. 5-12.

63. Grodzinski, P., et al., *A Modular Microfluidic System for Cell Pre-concentration and Genetic Sample Preparation.* Biomedical Microdevices, 2003. **5**(4): p. 303-310.

64. Gascoyne, P., et al., *Microsample preparation by dielectrophoresis: isolation of malaria.* Lab on a Chip, 2002. **2**(2): p. 70-75.

65. Colter, D.C., I. Sekiya, and D.J. Prockop, *Identification of a subpopulation of rapidly self-renewing and multipotential adult stem cells in colonies of human marrow stromal cells.* Proceedings of the National Academy of Sciences of the United States of America, 2001. **98**(14): p. 7841-7845.

66. Racila, E., et al., *Detection and characterization of carcinoma cells in the blood.* Proceedings of the National Academy of Sciences of the United States of America, 1998. **95**(8): p. 4589-4594.

67. Becker, F.F., et al., *Separation of human breast cancer cells from blood by differential dielectric affinity.* Proceedings of the National Academy of Sciences of the United States of America, 1995. **92**(3): p. 860-864.

68. Smerage, J.B. and D.F. Hayes, *The measurement and therapeutic implications of circulating tumour cells in breast cancer.* Br J Cancer, 2005. **94**(1): p. 8-12.

69. Cristofanilli, M., et al., *Circulating Tumor Cells: A Novel Prognostic Factor for Newly Diagnosed Metastatic Breast Cancer.* Journal of Clinical Oncology, 2005. **23**(7): p. 1420-1430.

70. Gaforio, J.-J., et al., *Detection of breast cancer cells in the peripheral blood is positively correlated with estrogen-receptor status and predicts for poor prognosis.* International Journal of Cancer, 2003. **107**(6): p. 984-990.

71. Allard, W.J., et al., *Tumor Cells Circulate in the Peripheral Blood of All Major Carcinomas but not in Healthy Subjects or Patients With Nonmalignant Diseases.* Clinical Cancer Research, 2004. **10**(20): p. 6897-6904.

72. Butler, T.P. and P.M. Gullino, *Quantitation of Cell Shedding into Efferent Blood of Mammary Adenocarcinoma.* Cancer Research, 1975. **35**(3): p. 512-516.

73. Liotta, L.A., J. Kleinerman, and G.M. Saldel, *The Significance of Hematogenous Tumor Cell Clumps in the Metastatic Process.* Cancer Research, 1976. **36**(3): p. 889-894.

74. Baret, J.-C., et al., *Fluorescence-activated droplet sorting (FADS): efficient microfluidic cell sorting based on enzymatic activity.* Lab on a Chip, 2009. **9**(13): p. 1850-1858.

75. Fu, A.Y., et al., *A microfabricated fluorescence-activated cell sorter.* Nature Biotechnology, 1999. **17**(11): p. 1109-1111.

76. Herzenberg, L.A., et al., *The History and Future of the Fluorescence Activated Cell Sorter and Flow Cytometry: A View from Stanford.* Clin Chem, 2002. **48**(10): p. 1819-1827.

77. Kruger, J., et al., *Development of a microfluidic device for fluorescence activated cell sorting.* Journal of Micromechanics and Microengineering, 2002. **12**(4): p. 486-494.

78. Adams, J.D., U. Kim, and H.T. Soh, *Multitarget magnetic activated cell sorter.* Proceedings of the National Academy of Sciences, 2008. **105**(47): p. 18165-18170.

79. Berger, M., et al., *Design of a microfabricated magnetic cell separator.* ELECTROPHORESIS, 2001. **22**(18): p. 3883-3892.

80. Gassei, K., et al., *Magnetic activated cell sorting allows isolation of spermatogonia from adult primate testes and reveals distinct GFRa1-positive subpopulations in men.* Journal of Medical Primatology, 2010. **39**(2): p. 83-91.

81. Miltenyi, S., et al., *High gradient magnetic cell separation with MACS.* Cytometry, 1990. **11**(2): p. 231-238.

82. Richard E, Z., et al., *Immunomagnetic Cell Enrichment Detects more Disseminated Cancer Cells than Immunocytochemistry in Vitro* The Journal of urology, 2000. **164**(5): p. 1834-1837.

83. Frühauf, N.R., et al., *Filtration of malignant cells: tumour cell depletion in an ex vivo model using a leukocyte adhesion filter.* Perfusion, 2001. **16**(1 suppl): p. 51-55.

84. Vona, G., et al., *Isolation by size of epithelial tumor cells - A new method for the immunomorphological and molecular characterization of circulating tumor cells.* American Journal of Pathology, 2000. **156**(1): p. 57-63.

85. Bhagat, A., et al., *Microfluidics for cell separation.* Medical and Biological Engineering and Computing, 2010. **48**(10): p. 999-1014.

86. Chang, W.C., L.P. Lee, and D. Liepmann, *Biomimetic technique for adhesion-based collection and separation of cells in a microfluidic channel.* Lab on a Chip, 2005. **5**(1): p. 64-73.

87. Chen, X., et al., *Microfluidic chip for blood cell separation and collection based on crossflow filtration.* Sensors and Actuators B: Chemical, 2008. **130**(1): p. 216-221.

88. Lien, K.-Y., et al., *Rapid isolation and detection of cancer cells by utilizing integrated microfluidic systems.* Lab on a Chip, 2010. **10**(21): p. 2875-2886.

89. Nagrath, S., et al., *Isolation of rare circulating tumour cells in cancer patients by microchip technology*. Nature, 2007. **450**(7173): p. 1235-1239.

90. El-Ali, J., P.K. Sorger, and K.F. Jensen, *Cells on chips.* Nature, 2006. **442**(7101): p. 403-411.

91. Toner, M. and D. Irimia, *Blood-on-a-chip.* Annual Review of Biomedical Engineering, 2005. **7**: p. 77-103.

92. Gardiner, K., *Pulsed field gel-electrophoresis.* Analytical Chemistry, 1991. **63**(7): p. 658-665.

93. Meldrum, D.R., *Sequencing genomes and beyond.* Science, 2001. **292**(5516): p. 515-517.

94. Nasmyth, K., *Segregating sister genomes: The molecular biology of chromosome separation.* Science, 2002. **297**(5581): p. 559-565.

95. Dunham, I., et al., *The DNA sequence of human chromosome 22.* Nature, 1999. **402**(6761): p. 489-495.

96. Sun, T.Q., D.A. Fenstermacher, and J.M.H. Vos, *Human artificial episomal chromosomes for cloning large dna fragments in human-cells.* Nature Genetics, 1994. **8**(1): p. 33-41.

97. Zolan, M.E., *Chromosome-length polymorphism in fungi.* Microbiological Reviews, 1995. **59**(4): p. 686-698.

98. Schwartz, D.C. and C.R. Cantor, *Separation of yeast chromosome-sized dnas by pulsed field gradient gel-electrophoresis.* Cell, 1984. **37**(1): p. 67-75.

99. Sudor, J. and M.V. Novotny, *Separation of large dna fragments by capillary electrophoresis under pulsed-field conditions.* Analytical Chemistry, 1994. **66**(15): p. 2446-2450.

100. Stein, D., et al., *Pressure-driven transport of confined DNA polymers in fluidic channels.* Proceedings of the National Academy of Sciences of the United States of America, 2006. **103**(43): p. 15853-15858.

101. Lubensky, D.K. and D.R. Nelson, *Single molecule statistics and the polynucleotide unzipping transition.* Physical Review E, 2002. **65**(3): p. 031917.

102. Smith, S.B. and A.J. Bendich, *Electrophoretic charge-density and persistence length of dna as measured by fluorescence microscopy*. Biopolymers, 1990. **29**(8-9): p. 1167-1173.

103. Dimarzio, E.A. and C.M. Guttman, *Peeling a polymer from a surface or from a line.* Journal of Chemical Physics, 1991. **95**(2): p. 1189-1197.

104. SantaLucia, J., H.T. Allawi, and A. Seneviratne, *Improved nearest-neighbor parameters for predicting DNA duplex stability*. Biochemistry, 1996. **35**(11): p. 3555-3562.

105. Gao, L., et al., *Separation of long DNA molecules through cleavage of hydrogen bonds under a stretching force.* Applied Physics Letters, 2007. **91**(11): p. 113902.

106. Cantor, C.R., C.L. Smith, and M.K. Mathew, *Pulsed-Field Gel Electrophoresis of Very Large DNA Molecules.* Annual Review of Biophysics and Biophysical Chemistry, 1988. **17**(1): p. 287-304.

107. Cohen, A.S., et al., *Rapid separation and purification of oligonucleotides by high-performance capillary gel-electrophoresis.* Proceedings of the National Academy of Sciences of the United States of America, 1988. **85**(24): p. 9660-9663.

108. Karger, B.L., Y.H. Chu, and F. Foret, *Capillary electrophoresis of proteins and nucleic-acids.* Annual Review of Biophysics and Biomolecular Structure, 1995. **24**: p. 579-610.

109. Kim, Y.S. and M.D. Morris, *Rapid pulsed-field capillary electrophoretic separation of megabase nucleic-acids.* Analytical Chemistry, 1995. **67**(5): p. 784-786.

110. Salieb-Beugelaar, G.B., et al., *Electrophoretic separation of DNA in gels and nanostructures.* Lab on a Chip, 2009. **9**(17): p. 2508-2523.

111. Zhao, S.-L., et al., *Gaussian fluctuations in tethered DNA chains.* The Journal of Chemical Physics, 2011. **134**(6): p. 065103.

112. Sosnowski, R.G., et al., *Rapid determination of single base mismatch mutations in DNA hybrids by direct electric field control.* Proceedings of the National Academy of Sciences, 1997. **94**(4): p. 1119-1123.

113. Wu, J., et al., *Separation of single-stranded DNA fragments at a 10-nucleotide resolution by stretching in microfluidic channels.* Lab on a Chip, 2011. **11**(23): p. 4036-4040.

114. Perkins, T.T., et al., *Stretching of a Single Tethered Polymer in a Uniform Flow.* Science, 1995. **268**(5207): p. 83-87.

115. Gosse, C. and V. Croquette, *Magnetic Tweezers: Micromanipulation and Force Measurement at the Molecular Level.* Biophysical journal, 2002. **82**(6): p. 3314-3329.

116. Smith, S., L. Finzi, and C. Bustamante, *Direct mechanical measurements of the elasticity of single DNA molecules by using magnetic beads.* Science, 1992. **258**(5085): p. 1122-1126.

117. Bustamante, C., Z. Bryant, and S.B. Smith, *Ten years of tension: single-molecule DNA mechanics.* Nature, 2003. **421**(6921): p. 423-427.

118. Wang, M.D., et al., *Stretching DNA with optical tweezers.* Biophysical journal, 1997. **72**(3): p. 1335-1346.

119. Cluzel, P., et al., *DNA: An Extensible Molecule.* Science, 1996. **271**(5250): p. 792-794.

120. Erdmann, M., et al., *Electrically controlled DNA adhesion.* Nature Nanotechnology, 2010. **5**(2): p. 154-159.

121. Rief, M., H. Clausen-Schaumann, and H.E. Gaub, *Sequence-dependent mechanics of single DNA molecules.* Nature Structural & Molecular Biology, 1999. **6**(4): p. 346-349.

122. Rant, U., et al., *Dynamic Electrical Switching of DNA Layers on a Metal Surface.* Nano Letters, 2004. **4**(12): p. 2441-2445.

123. Rant, U., et al., *Switchable DNA interfaces for the highly sensitive detection of label-free DNA targets.* Proceedings of the National Academy of Sciences, 2007. **104**(44): p. 17364-17369.

124. Rant, U., et al., *Detection and Size Analysis of Proteins with Switchable DNA Layers.* Nano Letters, 2009. **9**(4): p. 1290-1295.

125. Heaton, R.J., A.W. Peterson, and R.M. Georgiadis, *Electrostatic surface plasmon resonance: Direct electric field-induced hybridization and denaturation in monolayer nucleic acid films and label-free discrimination of base mismatches.* Proceedings of the National Academy of Sciences, 2001. **98**(7): p. 3701-3704.

126. Wong, I.Y. and N.A. Melosh, *Directed Hybridization and Melting of DNA Linkers using Counterion-Screened Electric Fields.* Nano Letters, 2009. **9**(10): p. 3521-3526.

127. Kaiser, W. and U. Rant, *Conformations of End-Tethered DNA Molecules on Gold Surfaces: Influences of Applied Electric Potential, Electrolyte Screening, and Temperature.* Journal of the American Chemical Society, 2010. **132**(23): p. 7935-7945.

128. Murphy, J.N., et al., *On the Nature of DNA Self-Assembled Monolayers on Au: Measuring Surface Heterogeneity with Electrochemical in Situ Fluorescence Microscopy.* Journal of the American Chemical Society, 2009. **131**(11): p. 4042-4050.

129. Spuhler, P.S., et al., *Platform for in situ real-time measurement of protein-induced conformational changes of DNA.* Proceedings of the National Academy of Sciences, 2010. **107**(4): p. 1397-1401.

130. Russel, W.B., D.A. Saville, and W.R. Schowalter, *Colloidal Dispersions*1992: Cambridge University Press.

131. Schoch, R.B., J. Han, and P. Renaud, *Transport phenomena in nanofluidics.* Reviews of Modern Physics, 2008. **80**(3): p. 839-883.

132. Vainrub, A. and B.M. Pettitt, *Thermodynamics of association to a molecule immobilized in an electric double layer.* Chemical Physics Letters, 2000. **323**(1-2): p. 160-166.

133. Herne, T.M. and M.J. Tarlov, *Characterization of DNA Probes Immobilized on Gold Surfaces.* Journal of the American Chemical Society, 1997. **119**(38): p. 8916-8920.

134. Steel, A.B., T.M. Herne, and M.J. Tarlov, *Electrochemical Quantitation of DNA Immobilized on Gold.* Analytical Chemistry, 1998. **70**(22): p. 4670-4677.

135. Schildkraut, C. and S. Lifson, *Dependence of the melting temperature of DNA on salt concentration.* Biopolymers, 1965. **3**(2): p. 195-208.

136. Tan, Z.-J. and S.-J. Chen, *Nucleic Acid Helix Stability: Effects of Salt Concentration, Cation Valence and Size, and Chain Length.* Biophysical journal, 2006. **90**(4): p. 1175-1190.

137. Keyser, U.F., et al., *Direct force measurements on DNA in a solid-state nanopore.* Nature Physics, 2006. **2**(7): p. 473-477.

138. Zhang, J. and B.I. Shklovskii, *Effective charge and free energy of DNA inside an ion channel.* Physical Review E, 2007. **75**(2): p. 021906.

139. Jiang, T., Z.D. Li, and J.Z. Wu, *Structure and swelling of grafted polyelectrolytes: Predictions from a nonlocal density functional theory.* Macromolecules, 2007. **40**(2): p. 334-343.

140. Jiang, T. and J.Z. Wu, *Ionic effects in collapse of polyelectrolyte brushes.* Journal of Physical Chemistry B, 2008. **112**(26): p. 7713-7720.

141. Henderson, D., et al., *Density Functional Study of the Electric Double Layer Formed by a High Density Electrolyte.* Journal of Physical Chemistry B, 2011. **115**(44): p. 12911-12914.

142. Lee, J.W., et al., *Comparison of Molecular Dynamics with Classical Density Functional and Poisson-Boltzmann Theories of the Electric Double Layer in Nanochannels.* Journal of Chemical Theory and Computation, 2012. **8**(6): p. 2012-2022.

143. Strogryn, A., *Equations for calculating the dielectric constant of saline water.* IEEE Transactions on Microwave Theory and Techniques, 1971. **MTT-19**(8): p. 733-736.

144. Zimm, B.H. and M. Lebret, *Counterion Condensation and System Dimensionality.* Journal of Biomolecular Structure & Dynamics, 1983. **1**(2): p. 461-471.

145. Ambia-Garrido, J., A. Vainrub, and B.M. Pettitt, *A model for structure and thermodynamics of ssDNA and dsDNA near a surface: A coarse grained approach.* Computer Physics Communications, 2010. **181**(12): p. 2001-2007.

146. Ding, F., et al., *Single-molecule mechanical identification and sequencing.* Nature Methods, 2012. **9**(4): p. 367-372.

147. Douglas, G.C. and B.F. King, *Isolation of pure villous cytotrophoblast from term human placenta using immunomagnetic microspheres.* Journal of Immunological Methods, 1989. **119**(2): p. 259-268.

148. Herr, J.K., et al., *Aptamer-Conjugated Nanoparticles for Selective Collection and Detection of Cancer Cells.* Analytical Chemistry, 2006. **78**(9): p. 2918-2924.

149. Kuhara, M., et al., *Magnetic cell separation using antibody binding with protein a expressed on bacterial magnetic particles.* Analytical Chemistry, 2004. **76**(21): p. 6207-6213.

150. Lewin, M., et al., *Tat peptide-derivatized magnetic nanoparticles allow in vivo tracking and recovery of progenitor cells.* Nature Biotechnology, 2000. **18**(4): p. 410-414.

151. Miltenyi, S., et al., *High-gradient magnetic cell-separation with macs.* Cytometry, 1990. **11**(2): p. 231-238.

152. Safarik, I. and M. Safarikova, *Use of magnetic techniques for the isolation of cells.* Journal of Chromatography B, 1999. **722**(1-2): p. 33-53.

153. Chalmers, J.J., et al., *Quantification of non-specific binding of magnetic micro- and nanoparticles using cell tracking velocimetry: Implication for magnetic cell separation and detection.* Biotechnology and Bioengineering, 2010. **105**(6): p. 1078-1093.

154. Kodituwakku, A.P., et al., *Isolation of antigen-specific B cells.* Immunol Cell Biol, 2003. **81**(3): p. 163-170.

155. Talasaz, A.H., et al., *Isolating highly enriched populations of circulating epithelial cells and other rare cells from blood using a magnetic sweeper device.* Proceedings of the National Academy of Sciences, 2009. **106**(10): p. 3970-3975.

156. Fujishige, S., K. Kubota, and I. Ando, *Phase-transition of aqueous-solutions of poly(N-isopropylacrylamide) and poly(N-isopropylmethacrylamide).* Journal of Physical Chemistry, 1989. **93**(8): p. 3311-3313.

157. Heskins, M. and J.E. Guillet, *Solution properties of poly(N-isopropylacrylamide).* Journal of Macromolecular Science: Part A - Chemistry, 1968. **2**(8): p. 1441-1455.

158. Schild, H.G., *Poly (N-Isopropylacrylamide) - Experiment, Theory and Application.* Progress in Polymer Science, 1992. **17**(2): p. 163-249.

159. Cooperstein, M.A. and H.E. Canavan, *Biological Cell Detachment from Poly(N-isopropyl acrylamide) and Its Applications.* Langmuir, 2009. **26**(11): p. 7695-7707.

160. Furukawa, H., et al., *Affinity selection of target cells from cell surface displayed libraries: a novel procedure using thermo-responsive magnetic nanoparticles.* Applied Microbiology and Biotechnology, 2003. **62**(5): p. 478-483.

161. Okamura, A., et al., *Poly(N-isopropylacrylamide)-graft-polypropylene membranes containing adsorbed antibody for cell separation.* Biomaterials, 2005. **26**(11): p. 1287-1292.

162. Kondo, A., H. Kamura, and K. Higashitani, *Development and application of thermo-sensitive magnetic immunomicrospheres for antibody purification.* Applied Microbiology and Biotechnology, 1994. **41**(1): p. 99-105.

163. Shamim, N., et al., *Thermosensitive polymer coated nanomagnetic particles for separation of bio-molecules.* Separation and Purification Technology, 2007. **53**(2): p. 164-170.

164. Yoshizako, K., et al., *Regulation of Protein Binding toward a Ligand on Chromatographic Matrixes by Masking and Forced-Releasing Effects Using Thermoresponsive Polymer.* Analytical Chemistry, 2002. **74**(16): p. 4160-4166.

165. Mori, T., D. Umeno, and M. Maeda, *Sequence-specific affinity precipitation of oligonucleotide using poly(N-isopropylacrylamide)–oligonucleotide conjugate.* Biotechnology and Bioengineering, 2001. **72**(3): p. 261-268.

166. Rahman, M.M. and A. Elaissari, *Temperature and magnetic dual responsive microparticles for DNA separation.* Separation and Purification Technology, 2011. **81**(3): p. 286-294.

167. Nagase, K., et al., *Preparation of Thermoresponsive Anionic Copolymer Brush Surfaces for Separating Basic Biomolecules.* Biomacromolecules, 2009. **11**(1): p. 215-223.

168. Hu, Y., et al., *Synthesis and characterization of chitosan-poly(acrylic acid) nanoparticles.* Biomaterials, 2002. **23**(15): p. 3193-3201.

169. Lee, D.H., R.A. Condrate, and J.S. Reed, *Infrared spectral investigation of polyacrylate adsorption on alumina.* Journal of Materials Science, 1996. **31**(2): p. 471-478.

170. Li, H. and C.P. Tripp, *Infrared Study of the Interaction of Charged Silica Particles with TiO2 Particles Containing Adsorbed Cationic and Anionic Polyelectrolytes.* Langmuir, 2005. **21**(6): p. 2585-2590.

171. Frey, W., D.E. Meyer, and A. Chilkoti, *Dynamic Addressing of a Surface Pattern by a Stimuli-Responsive Fusion Protein.* Advanced Materials, 2003. **15**(3): p. 248-251.

172. Gil, E.S. and S.M. Hudson, *Stimuli-reponsive polymers and their bioconjugates.* Progress in Polymer Science, 2004. **29**(12): p. 1173-1222.

173. Rzaev, Z.M.O., S. Dincer, and E. Piskin, *Functional copolymers of N-isopropylacrylamide for bioengineering applications.* Progress in Polymer Science, 2007. **32**(5): p. 534-595.

174. Mart, R.J., et al., *Peptide-based stimuli-responsive biomaterials.* Soft Matter, 2006. **2**(10): p. 822-835.

175. Urry, D.W., et al., *Hydrophobicity scale for proteins based on inverse temperature transitions.* Biopolymers, 1992. **32**(9): p. 1243-1250.

176. Yamaoka, T., et al., *Mechanism for the Phase Transition of a Genetically Engineered Elastin Model Peptide (VPGIG)40 in Aqueous Solution.* Biomacromolecules, 2003. **4**(6): p. 1680-1685.

177. Hyun, J., et al., *Capture and Release of Proteins on the Nanoscale by Stimuli-Responsive Elastin-Like Polypeptide "Switches".* Journal of the American Chemical Society, 2004. **126**(23): p. 7330-7335.

178. Meyer, D.E. and A. Chilkoti, *Purification of recombinant proteins by fusion with thermally-responsive polypeptides.* Nature Biotechnology, 1999. **17**(11): p. 1112.

179. Nath, N. and A. Chilkoti, *Fabrication of a Reversible Protein Array Directly from Cell Lysate Using a Stimuli-Responsive Polypeptide.* Analytical Chemistry, 2003. **75**(4): p. 709-715.

180. Gao, D., et al., *Fabrication of Antibody Arrays Using Thermally Responsive Elastin Fusion Proteins.* Journal of the American Chemical Society, 2005. **128**(3): p. 676-677.

181. Kim, J.-Y., A. Mulchandani, and W. Chen, *Temperature-triggered purification of antibodies.* Biotechnology and Bioengineering, 2005. **90**(3): p. 373-379.

182. Kim, J.-Y., et al., *Genetically Engineered Elastin-Protein A Fusion as a Universal Platform for Homogeneous, Phase-separation Immunoassay.* Analytical Chemistry, 2005. **77**(8): p. 2318-2322.